

AN INFORMATION-THEORETIC APPROACH TO DIVERSITY EVALUATION OF PROMPT-BASED GENERATIVE MODELS

Anonymous authors

Paper under double-blind review

ABSTRACT

Text-conditioned generation models are commonly evaluated based on the quality of the generated data and its alignment with the input text prompt. On the other hand, several applications of prompt-based generative models require sufficient diversity in the generated data to ensure the models' capability of generating image and video samples possessing a variety of features. However, the existing diversity metrics are designed for unconditional generative models, and thus cannot distinguish the diversity arising from variations in text prompts and that contributed by the generative model itself. In this work, our goal is to quantify the prompt-induced and model-induced diversity in samples generated by prompt-based models. Specifically, we propose the application of matrix-based information measures to address this task, decomposing the kernel-based entropy $H(X)$ of generated data X into the sum of conditional entropy $H(X|T)$, given text variable T , and mutual information $I(X; T)$. We show that this information-theoretic approach decomposes the existing Vendi diversity score defined based on $H(X)$ into the product of the following two terms: 1) *Conditional-Vendi* score based on $H(X|T)$ to quantify the model-induced diversity, and 2) *Information-Vendi* score based on $I(X; T)$ to measure the statistical relevance between X and prompt T . Our theoretical results provide an interpretation for this diversity quantification and show that the Conditional-Vendi score aggregates the Vendi scores within the modes of a mixture prompt distribution. We conduct several numerical experiments to show the correlation between the Conditional-Vendi score and the internal diversity of text-conditioned generative models.

1 INTRODUCTION

Prompt-based generative models, including text-to-image and text-to-video generation schemes, are widely used in various artificial intelligence (AI) applications. In prompt-based generative AI, the sample creation process begins with a text input and produces a random output aligned with that text. The conditional nature of this sample generation distinguishes prompt-based generative models from standard unconditional generative models where the objective is to produce samples distributed similarly to real data without any guiding input prompt. Since most evaluation metrics for generative models had been developed for unconditional models in the previous decade, the recent literature has sought to create scores tailored specifically for text-conditioned generative models.

The existing evaluation metrics for prompt-based generative models typically focus on fidelity and relevance in sample generation, i.e., they assess the visual quality of the produced samples and their alignment with the input prompt. Relevance is often measured by calculating a similarity score between a shared embedding of the text and image samples, e.g. in ClipScore (Hessel et al., 2021) which utilizes the CLIP embeddings of text and image data. Such shared embedding-based evaluation mechanisms have been further adapted to quantify the aesthetics, semantic consistency, and compositional accuracy of the generated data based on the input text prompt.

On the other hand, the diversity performance of prompt-based generative models has not been exclusively studied in the literature. The diversity scores proposed for unconditional generative models, such as Recall (Sajjadi et al., 2018; Kynkäänniemi et al., 2019), Coverage (Naeem et al., 2020),

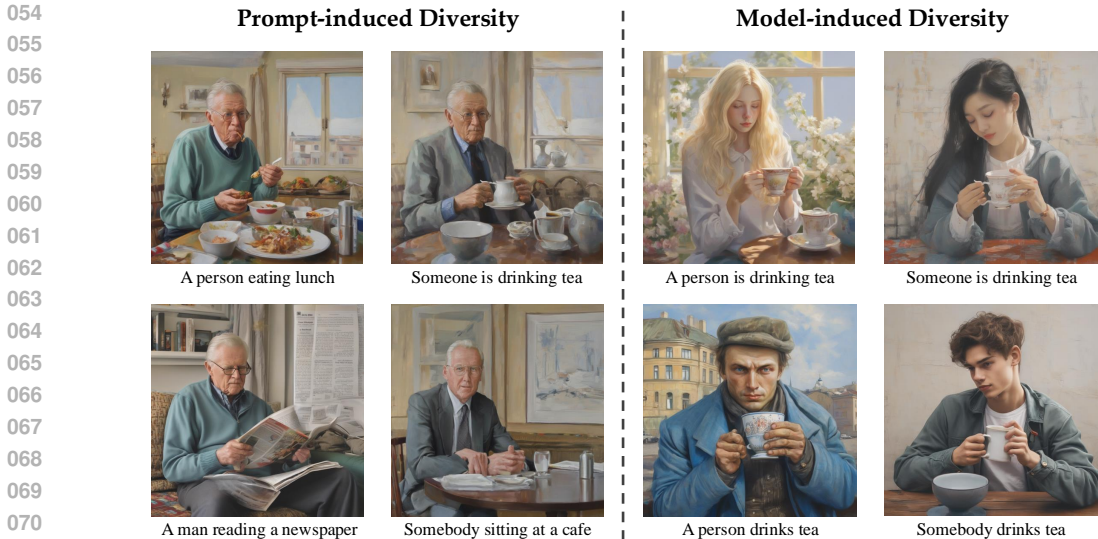


Figure 1: Illustration of *prompt-induced diversity*, where the diversity of generated images follows the variety of prompts and has little variation in other details, vs. *model-induced diversity*, where the diversity of images for similar prompts is due to the generation model.

Vendi (Friedman & Dieng, 2023; Pasarkar & Dieng, 2024), and RKE (Jalali et al., 2023), are often applied to quantify the variety of generated samples. However, in text-based generative models, the generated samples are typically produced in response to different input prompts, where the variation in input texts can significantly contribute to the diversity of the generated image or video samples. Thus, the diversity of data produced by prompt-based models is influenced by two main factors: 1) the variety of input prompts, and 2) the internal diversity of the model introducing randomness into the output samples. Figure 1 illustrates examples of prompt-induced diversity, where the variety of generated images is mostly due to the different prompts and the generated data has little variety in other details (images of similar people with similar poses), and model-induced diversity where the details not specified by the prompts vary significantly between generated images. This decomposition of diversity in text-based generative models has not been studied in the existing literature on conditional generative models including text-based image and video generation.

In this work, we focus on quantifying the two diversity components mentioned for prompt-based generative models. To this end, we propose an information-theoretic decomposition of the diversity of the model’s output data, X . The proposed decomposition is based on a classical identity in information theory, which shows that for variables X and T , the Shannon entropy $H(X)$, representing the uncertainty of X , can be decomposed into two terms as follows:

$$H(X) = H(X|T) + I(X; T)$$

Here, $H(X|T)$ denotes the conditional entropy of data X given the text variable T , which we interpret as the internal diversity of the text-based generative model not caused by variation in the input text T . Furthermore, the mutual information term $I(X; T)$ can be viewed as a measure of statistical relevance between the text T and the generated data X , quantifying how much information the model’s output conveys about the input text.

To mathematically define the entropy-based scores, we follow the kernel-matrix-based entropy definition, which has been applied by (Friedman & Dieng, 2023; Jalali et al., 2023; Pasarkar & Dieng, 2024) to unconditional generative models. These references apply the matrix-based entropy in quantum information theory, that is the entropy of the eigenvalues of the kernel matrix of generated data X , to measure the diversity of an unconditional model’s generated data. To extend the framework to conditional prompt-based generative models, we utilize the definition of matrix-based conditional entropy proposed by Giraldo et al. (2014). This work provides a definition for the conditional entropy of two general positive semi-definite matrices, which we select to be the kernel matrices of generated data X and text T . Following these definitions, our work extends the entropy-based approach in (Friedman & Dieng, 2023; Jalali et al., 2023) to conditional generative models. We de-

fine the *Conditional-Vendi* and *Information-Vendi* scores which decompose the unconditional Vendi score to model-induced and prompt-induced diversity measures.

To statistically interpret the defined scores, we derive the statistic estimated by the proposed scores from empirical generated samples. We show how the target statistic can be formulated in terms of the kernel covariance matrix of the Kronecker product of text T and data X vectors. **Importantly, we prove a theorem to interpret and provide an operational meaning for the proposed entropy-based scores.** Note that the conditional entropy measures in (Giraldo et al., 2014) do not follow standard information theory, and hence the defining equation $H(X, T) - H(T) = \mathbb{E}_{t \sim P_T}[H(X|T = t)]$, well-known for Shannon conditional entropy, does not hold for the conditional entropy measure in (Giraldo et al., 2014). To address this gap and provide a practical interpretation for the defined conditional entropy $H(X|T)$, we prove that under a mixture distribution P_T for text data with a hidden group variable G , the defined conditional entropy indeed aggregates $H(X|G = g)$ given prompt type $g \sim P_G$. This result shows the Conditional-Vendi is an aggregation of Vendi scores.

Specifically, our theoretical analysis on the connection between the Conditional VENDI score and average of unconditional entropy scores indicate a spectral approach to interpret the diversity evaluation of the proposed score. Following the spectral identification of modes in the eigendecomposition of matrix-based entropy function, we show that the modes used by the Conditional-VENDI score follow from the eigenvectors of the kernel covariance matrix of the text prompt distributions. Therefore, we visualize the diversity contributed by the prompt-based generative model using the spectral clustering of text samples according to the kernel function used in the definition of the diversity score. After computing the eigendirections of the text kernel matrix, we analyze the Hadamard product of each eigendirection-based rank-1 matrix and the joint (prompt,data) kernel matrix. This analysis reveals the variant clusters of images generated for each group of input text samples.

We numerically evaluate the proposed diversity scores for standard text-to-image, text-to-video, and image-captioning generative models. In our experiments, we simulate text-based generative models for which the ground-truth rankings of internal diversity and relevance are known. Our experimental results validate the consistency of our proposed information-theoretic scores and the ground-truth ranking of the models. We further decompose the Conditional-Vendi score across different modes of input text data, evaluating the models’ internal diversity across different types of input text. The following is a summary of the contributions of this work:

- Highlighting the diversity evaluation task in the context of conditional generative models,
- Proposing an information-theoretic framework for decomposing the diversity of generated data into prompt-induced and model-induced components to evaluate the internal diversity of prompt-based generative models
- **Providing an operational meaning for the defined scores and interpreting them as the average of entropy scores over the modes of a multi-modal text distribution**
- Presenting numerical results on the consistency between the conditional entropy score and the model-induced diversity of text-to-image and text-to-video generative models.

2 RELATED WORK

Evaluation of deep generative models: The existing metrics for the evaluation of generative models can be divided into reference-dependent and reference-free categories, as discussed in (Borji, 2022). As one type of reference-dependent metrics, a distance between generated and reference distributions is measured using metrics such as FID (Heusel et al., 2017) and KID (Bińkowski et al., 2018). Other reference-based metrics such as the Inception Score (Salimans et al., 2016), GAN-train/GAN-test (Shmelkov et al., 2018), Precision/Recall (Sajjadi et al., 2018; Kynkäänniemi et al., 2019), and Density/Coverage (Naem et al., 2020) are defined to quantify the diversity and quality of generated data in comparison to the samples in the real dataset. In addition, assessing memorization and novelty has been studied in several references, including the authenticity score (Alaa et al., 2022) and Feature Likelihood Divergence (Jiralerspong et al., 2023) to assess generalizability, and the rarity score (Han et al., 2023), KEN (Zhang et al., 2024) proposed to assess novelty. Note that the memorization metrics are inherently reference-based. In contrast, reference-free evaluations measure diversity and quality based only based on the generated data. Specifically, the Vendi (Friedman & Dieng, 2023; Pasarkar & Dieng, 2024) and RKE scores (Jalali et al., 2023) fall into this category.

Evaluation of conditional generative models: The evaluation of prompt-based generative models, including text-to-image and text-to-video models, has been studied in several related works. Most of the existing evaluation metrics attempt to measure the correlation between the prompt and the output. A standard metric for measuring the alignment of prompt and image is CLIPScore (Hessel et al., 2021), which measures the cosine similarity of the paired data using CLIP embedding. Some other works introduce different benchmarks and sets of prompts to evaluate different aspects. HEIM (Lee et al., 2023) assesses twelve aspects of the sample generation, including text-image alignment, image quality and bias. As noted by Astolfi et al. (2024), standard metrics focusing on style, aesthetics, and image quality, may overlook the diversity of images given a particular prompt. In their work, they measure diversity separately for each prompt using a similarity function and average the scores for the prompts. Kannen et al. (2024) follow a similar approach with the Vendi score. We note that both these methods require generating multiple images per prompt with different seeds to measure the score. On the other hand, our proposed Conditional-Vendi score does not require multiple sample generations per prompt and instead analyzes the types of text prompt in the assessment. Our theoretical results interpret Conditional-Vendi as an aggregation of the scores over text types.

Information measures for evaluating conditional generative models: Kim et al. (2022) utilize the mutual information (MI) between continuous text and image variables, and propose the Mutual Information Divergence (MID) score. This work fits a multivariate Gaussian distribution to the text and image data and then estimates their mutual information to quantify a relevance metric for conditional generative models. We note that our proposed Information-Vendi score is based on the matrix-based entropy score by Giraldo et al. (2014) which is different from the MI between Gaussian vectors fitted to the text and image data used in the MID score. Different from MID, Information-Vendi relies on kernel similarity values to identify a cluster variable for MI calculation.

3 PRELIMINARIES

Throughout the work, we focus on a conditional generative model that produces a data vector $X \in \mathcal{X}$ given an input text prompt $T \in \mathcal{T}$ according to a conditional distribution $P_{X|T}$, i.e., for text prompt $T = t$ the model outputs a random sample following $P_{X|T=t}$. We consider n sample pairs $(t_i, x_i) \sim P_T \times P_{X|T}$ where each text prompt t_i is drawn independently from the distribution P_T and then the generated sample x_i is generated according to $P_{X|T=t_i}$. Our goal is to quantify the internal diversity of the prompt-based generative model, influencing the variety of data generated x_1, \dots, x_n independently of the diversity of input texts t_1, \dots, t_n .

3.1 ENTROPY-BASED DIVERSITY SCORES FOR UNCONDITIONAL GENERATIVE MODELS

Consider generated samples $x_1, \dots, x_n \in \mathcal{X}$ following the distribution P_X of an unconditional generative model. For a kernel function $k : \mathcal{X} \times \mathcal{X} \rightarrow \mathbb{R}$, the kernel similarity matrix $K \in \mathbb{R}^{n \times n}$ is $K = [k(x_i, x_j)]_{1 \leq i, j \leq n}$. Following the standard definition, a kernel function k satisfies the positive semidefinite property (PSD), which means that the above kernel matrix will be PSD for any arbitrary selection of data points $x_1, \dots, x_n \in \mathcal{X}$, i.e., all its eigenvalues are non-negative. A popular kernel function is the Gaussian (RBF) kernel, which for a bandwidth parameter σ is defined as:

$$k(x, x') = \exp\left(\frac{-\|x - x'\|_2^2}{2\sigma^2}\right) \quad (1)$$

Assuming that a kernel function k is normalized, i.e. $k(x, x) = 1$ for every $x \in \mathbb{R}^d$, then the non-negative eigenvalues $\lambda_1, \dots, \lambda_n$ of $\frac{1}{n}K$ will add up to 1, implying that they represent a probability model. In the literature, Friedman & Dieng (2023); Jalali et al. (2023); Pasarkar & Dieng (2024) propose using the general-order- α Renyi entropy of the probability model as the model’s diversity score, defined as follows for $\frac{1}{n}K$:

$$H_\alpha(X) := H_\alpha\left(\frac{1}{n}K\right) = \frac{1}{1 - \alpha} \log\left(\sum_{i=1}^n \lambda_i^\alpha\right) \quad (2)$$

In the special case of $\alpha = 1$, the above definition results in the Shannon-entropy of eigenvalues $H_1\left(\frac{1}{n}K\right) = \sum_{i=1}^n \lambda_i \log(1/\lambda_i)$. Also, we note that the Vendi and RKE scores defined by Friedman & Dieng (2023); Pasarkar & Dieng (2024) are the exponential of the defined entropy measure, where

$$\text{Vendi}_\alpha(x_1, \dots, x_n) := \exp\left(H_\alpha\left(\frac{1}{n}K\right)\right) \quad (3)$$

To statistically interpret the entropy measures of the samples' kernel matrix, Bach (2022); Jalali et al. (2023) note that the normalized kernel matrix $\frac{1}{n}K$ shares the same non-zero eigenvalues with the empirical kernel covariance matrix \widehat{C}_X defined as:

$$\widehat{C}_X = \frac{1}{n} \sum_{i=1}^n \phi(X_i) \phi(X_i)^\top \quad (4)$$

Here, $\phi : \mathcal{X} \rightarrow \mathbb{R}^d$ denotes the kernel feature map satisfying the relation $k(x, x') = \langle \phi(x), \phi(x') \rangle$ for every $x, x' \in \mathcal{X}$ where $\langle \cdot, \cdot \rangle$ is the standard inner-product in the \mathbb{R}^d space. As a result, the entropy of the kernel matrix K 's eigenvalues equals the entropy of \widehat{C}_X . Note that \widehat{C}_X is the empirical estimation of the underlying kernel covariance matrix $C_X = \mathbb{E}_{X \sim P_X} [\phi(X) \phi(X)^\top]$.

3.2 MATRIX-BASED CONDITIONAL ENTROPY AND MUTUAL INFORMATION

In the previous subsection, we reviewed the standard definition of order- α matrix-based entropy for PSD matrices. Here, we discuss an extension proposed by Giraldo et al. (2014) to define matrix-based conditional entropy and mutual information for two variables $X \in \mathcal{X}$ and $T \in \mathcal{T}$. For variables X and T , we consider normalized kernel functions $k_X : \mathcal{X} \times \mathcal{X} \rightarrow \mathbb{R}$ and $k_T : \mathcal{T} \times \mathcal{T} \rightarrow \mathbb{R}$, where the kernel functions satisfy $k_X(x, x) = 1$ and $k_T(t, t) = 1$ for every input x and t . Given the two kernel functions, Giraldo et al. (2014) define the order- α matrix-based joint entropy $H_\alpha(X, T)$ as the order- α entropy of the PSD matrix $\frac{1}{n}K_X \odot K_T$, in which K_X and K_T are the kernel matrices of X and T samples and \odot denotes the entry-wise Hadamard product.

Note that the Hadamard product $K_X \odot K_T$ represents the kernel matrix of concatenated samples $[x_i, t_i]$, where we consider the kernel function $k_{X,T}([x, t], [x', t']) = k_X(x, x')k_T(t, t')$ to be the product of marginal kernel functions. This definition is sensible, since the joint similarity value, taking value over $[0, 1]$ in Gaussian kernels, is considered to be the multiplication of the similarity scores for the text and output data vectors. Then, Giraldo et al. (2014) propose defining conditional entropy $H_\alpha(X|T)$ as the difference between the joint and marginal entropy values:

$$H_\alpha(X|T) := H_\alpha(X, T) - H_\alpha(T) = H_\alpha\left(\frac{1}{n}K_X \odot K_T\right) - H_\alpha\left(\frac{1}{n}K_T\right) \quad (5)$$

Specifically, it is shown that the defined conditional entropy $H_\alpha(X|T)$ is non-negative for every normalized kernel function k_X and k_T . Furthermore, Giraldo et al. (2014) define the matrix-based mutual information $I_\alpha(X; T)$ as the difference between the defined conditional and marginal entropy which is shown to be non-negative given normalized kernel functions k_X and k_T :

$$I_\alpha(X; T) := H_\alpha(X) - H_\alpha(X|T) = H_\alpha\left(\frac{1}{n}K_X\right) + H_\alpha\left(\frac{1}{n}K_T\right) - H_\alpha\left(\frac{1}{n}K_X \odot K_T\right) \quad (6)$$

4 AN INFORMATION-THEORETIC DIVERSITY QUANTIFICATION FOR PROMPT-BASED GENERATIVE MODELS

We aim to extend the entropy-based diversity scores for unconditional generative models to conditional text-based generative models. Note that if we only evaluate the entropy score of the generated samples x_1, \dots, x_n , the evaluated score does not separate the diversity contributed by different prompts from the internal diversity of the model creating varying samples for similar prompts.

To separate out the effect of diverse input prompts on the variety of the generated samples $\mathbf{x}_1, \dots, \mathbf{x}_n$, we propose applying the conditional entropy as formulated by Giraldo et al. (2014) for a general quantum information-theoretic setting and propose the following *order- α Conditional-Vendi Score*:

$$\text{Conditional-Vendi}_\alpha(x_1, \dots, x_n | t_1, \dots, t_n) := \exp\left(H_\alpha\left(\frac{1}{n}K_X \odot K_T\right) - H_\alpha\left(\frac{1}{n}K_T\right)\right)$$

In the above, K_X and K_T denote the kernel matrices for the generated samples and input prompts, respectively. In addition to the proposed Conditional-Vendi score for measuring the internal diversity of the model, we propose the *Information-Vendi* score following the identity $I(X; T) = H(X) + H(T) - H(X, T)$ in standard information theory:

$$\text{Information-Vendi}_\alpha(x_1, \dots, x_n; t_1, \dots, t_n) := \exp\left(H_\alpha\left(\frac{1}{n}K_X\right) + H_\alpha\left(\frac{1}{n}K_T\right) - H_\alpha\left(\frac{1}{n}K_X \odot K_T\right)\right)$$

Note that the defined Conditional-Vendi $_{\alpha}$ and Information-Vendi $_{\alpha}$ lead to a decomposition of Vendi $_{\alpha}$ score (Pasarkar & Dieng, 2024) into the product of the following two terms:

$$\begin{aligned} \text{Vendi}_{\alpha}(x_1, \dots, x_n) &= \text{Conditional-Vendi}_{\alpha}(x_1, \dots, x_n | t_1, \dots, t_n) \\ &\quad \times \text{Information-Vendi}_{\alpha}(x_1, \dots, x_n; t_1, \dots, t_n). \end{aligned}$$

In the above, Vendi $_{\alpha}$ measures the diversity of generated data x_1, \dots, x_n , while the Conditional-Vendi $_{\alpha}$ score is a quantification of the internal diversity of the model that is not influenced by the variety of input prompts. Also, Information-Vendi $_{\alpha}$ can be viewed as a relevance score quantifying how the diversity of generated samples is statistically correlated with the diversity of text prompts. Therefore, the proposed decomposition leads to a mechanism for the internal diversity evaluation of conditional generative models.

5 STATISTICAL INTERPRETATION OF THE ENTROPY-BASED SCORES

In this section, we aim to statistically interpret the defined conditional diversity scores as the expectation of prompt-specific entropy $H(X|T = t)$. First, we derive the statistic estimated from empirical samples by the entropy-based scores, and then we connect the conditional entropy measure to the expectation of unconditional entropy values. According to the Schur product theorem, the Hadamard product $K_X \odot K_T$ of PSD kernel matrices K_X, K_T will also be a PSD kernel matrix. We note that the kernel matrix corresponds to the following feature map $\phi_{X,T} : \mathcal{X} \times \mathcal{T} \rightarrow \mathbb{R}^{d_x d_t}$ where \otimes denotes the Kronecker product:

$$\phi_{X,T}([x, t]) = \phi_X(x) \otimes \phi_T(t)$$

The above holds due to the identity $\langle \phi_{X,T}([x, t]), \phi_{X,T}([x', t']) \rangle = k_X(x, x') k_T(t, t')$. The following proposition formulates kernel-based conditional entropy and mutual information using $\phi_{X,T}$.

Proposition 1. *Consider the kernel matrices K_X for samples x_1, \dots, x_n and K_T for samples t_1, \dots, t_n . Then, $\frac{1}{n} K_X \odot K_T$ (used for defining joint entropy $H_{\alpha}(X, T)$) share the same non-zero eigenvalues with the following kernel covariance matrix:*

$$\widehat{C}_{X,T} := \frac{1}{n} \sum_{i=1}^n \phi_{X,T}([x_i, t_i]) \phi_{X,T}([x_i, t_i])^{\top} = \frac{1}{n} \sum_{i=1}^n \left[\phi_X(x_i) \phi_X(x_i)^{\top} \right] \otimes \left[\phi_T(t_i) \phi_T(t_i)^{\top} \right]$$

Corollary 1. *Consider the composite feature map $\phi_{X,T}$ and joint kernel covariance matrix $\widehat{C}_{X,T}$ defined above. Then, given marginal kernel covariance matrices $\widehat{C}_X = \frac{1}{n} \sum_{i=1}^n \phi_X(x_i) \phi_X(x_i)^{\top}$, $\widehat{C}_T = \frac{1}{n} \sum_{i=1}^n \phi_T(t_i) \phi_T(t_i)^{\top}$, the following holds for the defined conditional entropy and mutual information:*

$$H_{\alpha}(X|T) = H_{\alpha}(\widehat{C}_{X,T}) - H_{\alpha}(\widehat{C}_T), \quad I_{\alpha}(X;T) = H_{\alpha}(\widehat{C}_X) + H_{\alpha}(\widehat{C}_T) - H_{\alpha}(\widehat{C}_{X,T})$$

Proof. The proof is deferred to the Appendix. Note that Conditional-Vendi $_{\alpha}(x_1, \dots, x_n | t_1, \dots, t_n) = \exp(H_{\alpha}(X|T))$ and Information-Vendi $_{\alpha}(x_1, \dots, x_n; t_1, \dots, t_n) = \exp(I_{\alpha}(X;T))$ \square

Corollary 1 shows that given the underlying covariance matrices $C_X = \mathbb{E}_{x \sim P_X} [\phi_X(x) \phi_X(x)^{\top}]$, $C_T = \mathbb{E}_{t \sim P_T} [\phi_T(t) \phi_T(t)^{\top}]$, and $C_{X,T} = \mathbb{E}_{(x,t) \sim P_{X,T}} [\phi_{X,T}([x, t]) \phi_{X,T}([x, t])^{\top}]$, the defined entropy-based scores converge to the following statistics when the sample size n tends to infinity:

$$\widetilde{H}_{\alpha}(X|T) = H_{\alpha}(C_{X,T}) - H_{\alpha}(C_T), \quad \widetilde{I}_{\alpha}(X;T) = H_{\alpha}(C_X) + H_{\alpha}(C_T) - H_{\alpha}(C_{X,T}).$$

Note that the entropy-based statistic $H_{\alpha}(C_X)$ represents the statistic estimated by the logarithm of the Vendi score defined in (Friedman & Dieng, 2023).

Next, we prove that for a mixture text distribution P_T where the text variable follows random mode $G \in \{1, \dots, m\}$, the defined conditional entropy score aggregates the expectation of the unconditional entropy score $H(X|G = i)$ over the m text modes $1, \dots, m$.

Theorem 1. Consider the Gaussian kernel with bandwidth σ . Suppose T follows a mixture distribution $\sum_{i=1}^m \omega_i P_{T,i}$ where ω_i denotes the weight of the i th component $P_{T,i}$ with mean vector μ_i and total variance $\mathbb{E}_{T \sim P_{T,i}}[\|T - \mu_i\|_2^2] = \sigma_i^2$. Given the aggregation map $f(z) = \exp((1 - \alpha)z)$, for every order $\alpha \geq 2$, the matrix-based order- α conditional entropy satisfies the following inequality where $g(z) = \frac{\alpha}{\alpha-1} \log\left(\frac{1}{1-z/\|\omega\|_\alpha}\right)$ is an increasing scalar function with $g(0) = 0$:

$$\left| \tilde{H}_\alpha(X|T) - f^{-1}\left(\mathbb{E}_{T \sim \omega^\alpha} \left[f\left(\tilde{H}_\alpha(X|G = T)\right)\right]\right) \right| \leq 2g\left(32 \sum_{i=1}^k \omega_i \left[\frac{\sigma_i^2}{\sigma^2} + \sum_{j=1}^{i-1} \exp\left(-\frac{\|\mu_i - \mu_j\|_2^2}{\sigma^2}\right)\right]\right)$$

The above theorem shows that if the text samples come from m distinct modes satisfying $\frac{\|\mu_i - \mu_j\|_2}{\sigma} \gg 1$ for every $i \neq j$ and $\frac{\mathbb{E}_{P_{T,i}}[\|T - \mu_i\|_2^2]}{\sigma^2} \ll 1$, then the defined conditional entropy score $H(X|T)$ aggregates the unconditional entropy score $H(X|G = i)$ given the prompt group. Therefore, this result extends the expectation-based interpretation of Shannon conditional entropy to the matrix-based conditional entropy defined in Giraldo et al. (2014).

Based on Theorem 1, we propose a text-type-based diversity evaluation, where we restrict the evaluation of the prompt-based generative model to the prompts in the same group, i.e. the same mode in the mixture text distribution. To do this, we find the eigendirections corresponding to the text clusters by performing an eigendecomposition of text kernel matrix $\frac{1}{n}K_T = \sum_{i=1}^n \lambda_i v_i v_i^\top$ where $\lambda_1 \geq \dots \geq \lambda_n$ are the sorted eigenvalues and v_1, \dots, v_n are the sorted eigenvectors. Then, we note that the Hadamard product $\frac{1}{n}K_X \odot K_T$ used for joint entropy can be decomposed as: $\frac{1}{n}K_X \odot K_T = \sum_{i=1}^n \lambda_i (K_X \odot v_i v_i^\top)$. As a result, to evaluate the diversity of the generation model, we apply eigendecomposition to each $K_X \odot v_i v_i^\top$, where v_i marks the samples in group i , and find the sample indices with the maximum entries on the principal eigenvectors of $K_X \odot v_i v_i^\top$.

6 NUMERICAL RESULTS

We empirically evaluated the Conditional-Vendi and Information-Vendi scores for three types of conditional generative models: 1) text-to-image, 2) text-to-video generation, and 3) image-captioning models. For text-to-image models, we tested Flux (Lab, 2024), Stable Diffusion 2.1 (Rombach et al., 2022), Stable Diffusion XL (Podell et al., 2024), GigaGAN (Kang et al., 2023), Kandinsky (Razzhigaev et al., 2023), and PixArt (Chen et al., 2023b; 2024b). For prompt-based video generative models, we considered VideoCrafter1 (Chen et al., 2023a), Show-1 (Zhang et al., 2023), and Open-Sora (Zheng et al., 2024). For image-captioning models, we experimented with BLIP (Li et al., 2022), GIT (Wang et al., 2022), and GPT4o-mini (OpenAI, 2024).

Embeddings used in the evaluation of generative models. Unlike standard embedding-based scores for text-to-image models such as CLIPScore (Hessel et al., 2021), which require the same embedding model for the text and generated image, the definitions of Conditional-Vendi and Information-Vendi allow different feature extractors for text and generated sample. In our experiments, we followed (Stein et al., 2023; Kynkäänniemi et al., 2023), to use the DINOv2 (Oquab et al., 2023) embedding for image data. For text data, we used Gemini (Team, 2024) and CLIP (Radford et al., 2021), and for video samples, following the video evaluation literature (Kim et al., 2024; Saito et al., 2020; Unterthiner et al., 2019), we used I3D (Carreira & Zisserman, 2017). To select the bandwidth parameter σ , similar to (Jalali et al., 2023), we chose the Gaussian kernel bandwidth for each type of data as the smallest σ that ensures a variance below 0.01 in the evaluated score over independent evaluations. We observed that for image data, $\sigma \in [20, 30]$; for text data, $\sigma \in [0.1, 0.8]$; and for video data, $\sigma \in [10, 20]$ can satisfy this requirement.

Quantifying model-induced diversity via Conditional-Vendi. To illustrate how Conditional-Vendi correlates with the model-induced diversity, we considered a toy experiment with 10 different dog breeds from the ImageNet dataset (Deng et al., 2009) as simulated outputs for a text-to-image model. We generated two sets of prompts using GPT4o (OpenAI, 2024). In the first set, the breed of dog in the picture was not specified, while in the other one, the breed was explicitly mentioned. As shown in Figure 2, increasing the number of breeds sampled from the dataset led to the growth of the Vendi score, regardless of the text prompt. However, Conditional-Vendi only increased when the breed was not specified in the prompts, and in the second case where the breed had been included in the prompt, the score remained relatively constant, implying that the diversity in pictures

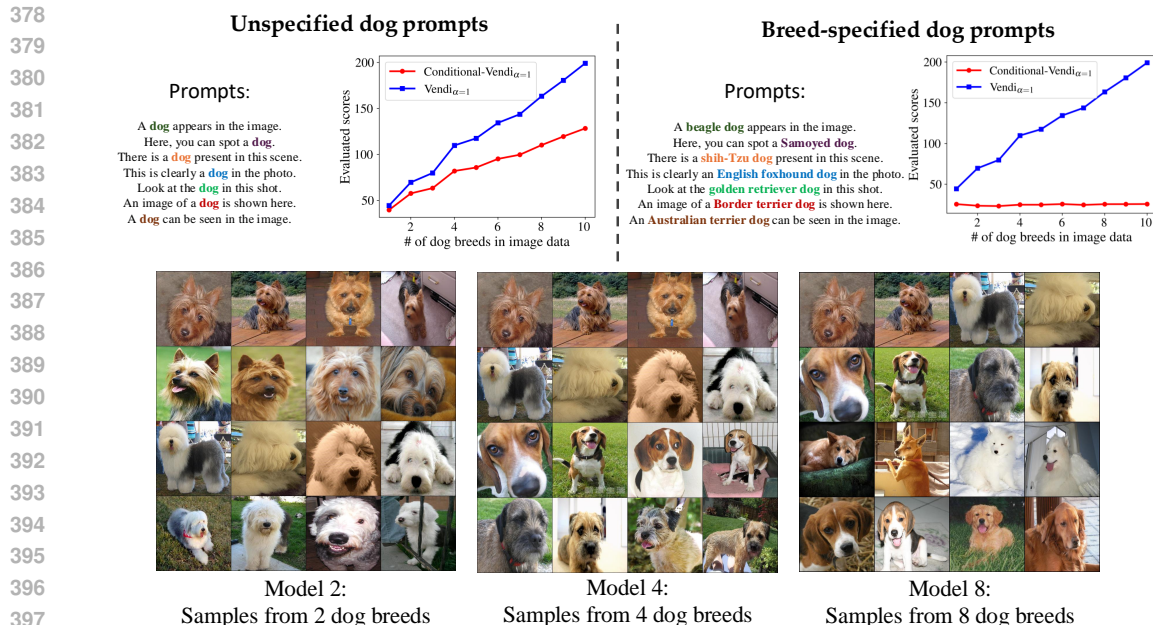


Figure 2: Evaluated Conditional-Vendi and Vendi scores on dog samples in the ImageNet dataset. (Left Plot): we simulated prompts on "dog" pictures without specifying the dog breed, (Right Plot) we added the breed information for dogs to the prompts.

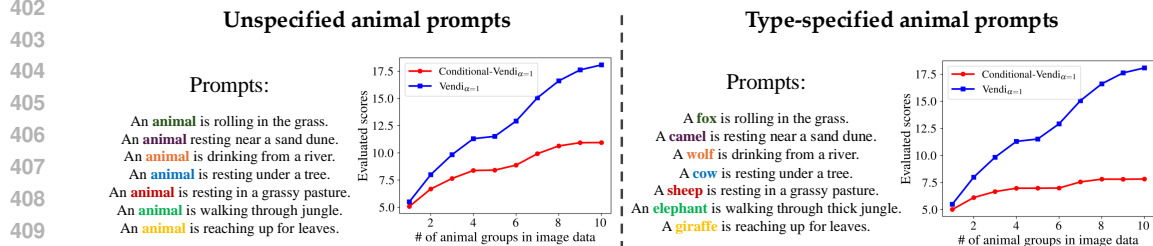


Figure 3: Evaluated Conditional-Vendi and Vendi scores on animal samples generated by Stable Diffusion-XL. (Left Plot): we do not specify the animal types in the prompt, (Right Plot) we specify the animal types in the prompt.

mostly follows the text prompt. To repeat this observation for text-to-image models, we considered 10 types of animals generated by Stable Diffusion XL, as shown in Figure 3. Similar to the previous experiment, we found that Conditional-Vendi increased at a more rapid rate when the prompts did not specify the type of animal in the picture. In contrast, when the animal types were specified in the prompts, there was only a slight increase in the Conditional-Vendi value.

Text-to-Image Model Evaluation: In Figure 4, we compared Flux, Stable Diffusion XL, GigaGAN, and Kandinsky. As shown in the plot, we generated 30,000 samples using each model, and then clustered the prompts into k groups, using k -means clustering on the Gemini embedding of text data, for different values of k . To simulate varying diversity across clusters, we assigned the image generated for the center of each cluster to all prompts within that cluster and measured the scores for different clusters. For example, when $k=2000$, we had 2,000 images for the k clusters, with the text in each cluster paired with one of the images. As k grows, we observed an increase in Information-Vendi, validating the fact that the images become more relevant to their prompts. Also, the Conditional-Vendi increased, as we expect the diversity of images to grow with more text clusters. Notably, while GigaGAN achieved a higher Vendi score, its Information-Vendi score was lower than that of SD-XL. This observation suggests that GigaGAN performs well at generating diverse outputs given prompts, but in terms of relevance, Flux and SD-XL are better. Our results align with conclusions made by Astolfi et al. (2024).

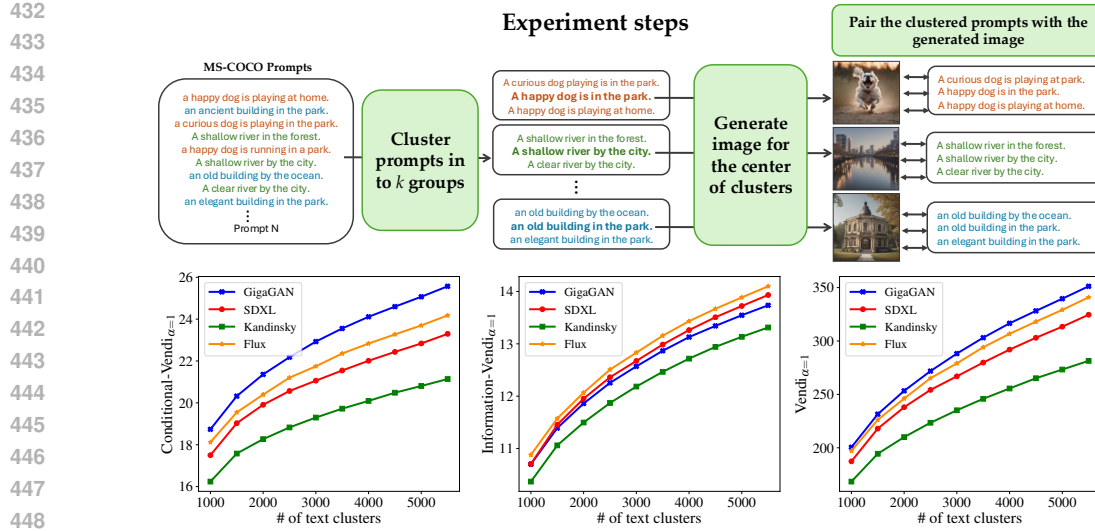


Figure 4: Comparing Conditional-Vendi and Information-Vendi of different text-to-image models.

Figure 5: Quantifying image diversity for different clusters of text prompts. Images are generated using the PixArt- α model.

Measuring Conditional-Vendi across prompt types. To measure Conditional-Vendi conditioned on the prompt type, we created 5000 prompts with different categories using GPT4o and generated the corresponding images with the text-to-image models. In Figure 5, top 2 groups of PixArt- α in terms of conditional entropy values are shown. We observed that "dog" text-based top 3 clusters of images looked more diverse than the image clusters for "airplane"-type prompts. Also, we evaluated Conditional-Vendi score of "dog" texts was significantly higher than that of the "airplane" class. We have tested other generative models in the appendix.

Text-to-Video Model Evaluation. For the experiments on video data, to ensure the fairness of our evaluation, we used VBench samples (Huang et al., 2024), which generated samples belong to the 8 content categories. In Figure 6, we used VideoCrafter-1, Show-1, and Open-Sora-1.2. We observed that VideoCrafter videos look less diverse and, in some cases, may not correlate significantly with the captions, when compared to Open-Sora. Confirming this observation, the Conditional-Vendi and Information-Vendi scores were lower for VideoCrafter than those for Open-Sora.

Image-Captioning Evaluation. For image captioning, we used 10 classes from the ImageNet dataset as input for BLIP-2, GIT and GPT4o-mini. In Figure 7, we compared captions for the top three groups of images: gas pump, church, and cassette player. GIT generated more diverse captions compared to BLIP, which was confirmed by the Conditional-Vendi scores. On the other hand, GPT4o-mini generated longer and more detailed captions compared to GIT, which was also reflected in the evaluated Conditional-Vendi and Information-Vendi scores.

	VideoCrafter-1	Show-1	Open-Sora-1.2
486			
487			
488	Caption Mode #1		
489	close up video of flower petals		
490	close up video of strawberry plant		
491	close up video of tree bark		
492	tree with golden leaves		
493	close up view of a plant		
494	Caption Mode #2		
495	close up shot of a wild bear		
496	a bear wearing red jersey		
497	close up video of snail		
498	an American crocodile		
499	close up of a lemur		
500	Caption Mode #3		
501	high angle shot of a clock tower		
502	close up shot of a steel structure		
503	an apartment building with balcony		
504	low angle shot of a building		
505	top view of a high rise building		
506	Evaluated Scores:	Cond-Vendi $_{\alpha=1}$ = 5.18 Info-Vendi $_{\alpha=1}$ = 3.13	Cond-Vendi $_{\alpha=1}$ = 6.45 Info-Vendi $_{\alpha=1}$ = 3.80
507			Cond-Vendi $_{\alpha=1}$ = 19.18 Info-Vendi $_{\alpha=1}$ = 9.18

Figure 6: Measuring Conditional-Vendi and Information-Vendi for text-to-video models

	BLIP-2	GIT	GPT4o-mini
508			
509	Image Mode #1		
510	a gas pump with three different colors.	a gas pump at a gas station with a red gas pump .	A vintage gas pump with a faded sign, displaying old pricing and a weathered metallic finish.
511	a gas pump with two different types of fuel.	a gas pump at a gas station in the middle of a road.	A man stands at a gas pump , holding a nozzle and filling two metal containers on a cart. He wears a black vest over a blue shirt and denim jeans, with a focused expression. In the background.
512	a man filling up his car at a gas station.	a woman in a white dress is filling up a car.	A vintage green gas pump stands in a grassy area, surrounded by trees and a white building in the background.
513	a woman filling up her car at a gas station.	a vintage gas station with a man filling up a gas pump.	
514	an old gas pump in front of a barn.	an old gas pump sitting in a field.	
515	an old gas pump in front of a house.	an old gas pump sitting in front of a building.	
516	Image Mode #2		
517	the inside of a church with wooden benches.	the interior of the cathedral of the holy trinity.	Interior of a spacious church featuring wooden pews, stained glass windows, and a decorative altar at end.
518	the interior of a church with wooden pews.	the interior of a church with stained windows.	a tall stone church with a pointed steeple and multiple spires, surrounded by a graveyard with weathered tombstones.
519	a church with a steeple and a graveyard	a small church with a steeple and a sign that says "catholic church".	a white church with a steeple, surrounded by dark clouds, with light one side of the building.
520	a church with a graveyard and a clock tower	a church with a stone roof and a graveyard.	
521	a white church with two steeple towers	a white church with a steeple and a blue sky.	
522	a white church with a red door and a fence	a white church with a steeple and steps.	
523	Image Mode #3		
524	a stereo system with a record player.	the stereo system is in the floor of the computer room.	a stereo system with two large speakers, a display panel in the center, and a remote control beside it.
525	a stereo system with a cassette player and a radio.	the radio is a stereo system that can be used to record or record a player.	a vintage boombox with a cassette tape deck and speakers, featuring various buttons and a handle on top.
526	a blue cassette player with headphones and a microphone.	the boombox is a compact cassette player that can be used as a microphone.	car dashboard displaying radio and climate control buttons, air vents above, and a textured surface around the controls
527	a silver portable cassette player with earphones.	sony's original sony audio cassette player.	
528	the interior of a car with a radio and dash	the radio is a compact car that can be used as a radio.	
529	a car radio with a digital display and buttons		
530	Evaluated Scores:	Cond-Vendi $_{\alpha=1}$ = 4.09 Info-Vendi $_{\alpha=1}$ = 2.28	Cond-Vendi $_{\alpha=1}$ = 10.9 Info-Vendi $_{\alpha=1}$ = 3.28
531			Cond-Vendi $_{\alpha=1}$ = 13.10 Info-Vendi $_{\alpha=1}$ = 3.98

Figure 7: Conditional-Vendi and Information-Vendi of image-captioning models for 3 image types

7 CONCLUSION

In this work, we proposed an evaluation score to measure the internal diversity of prompt-based generative models, isolating diversity that is not induced by variations in text prompts. The proposed method is based on a decomposition of unconditional matrix-based entropy scores, Vendi and RKE, into Conditional-Vendi and Information-Vendi components. From a theoretical perspective, we derived the kernel-based statistics estimated by these scores and demonstrated their connection to the expectation of unconditional entropy values given a fixed text prompt. In our experiments, we evaluated the proposed scores in multiple settings where the ground-truth ranking of model diversity and relevance was known, showing that the scores correlate well with the ground-truth rankings. A future direction is to apply the proposed scores to quantify biases in existing models regarding sample generation across different human ethnicities and genders. Additionally, using these scores as a regularization penalty to train more diverse prompt-based models is another interesting area for further exploration.

REFERENCES

- 540
541
542 Ahmed Alaa, Boris Van Breugel, Evgeny S Saveliev, and Mihaela van der Schaar. How faithful
543 is your synthetic data? sample-level metrics for evaluating and auditing generative models. In
544 *International Conference on Machine Learning*, pp. 290–306. PMLR, 2022.
- 545 Pietro Astolfi, Marlene Careil, Melissa Hall, Oscar Mañas, Matthew Muckley, Jakob Verbeek, Adri-
546 ana Romero Soriano, and Michal Drozdal. Consistency-diversity-realism pareto fronts of condi-
547 tional image generative models, 2024. URL <https://arxiv.org/abs/2406.10429>.
- 548 Francis R. Bach. Information theory with kernel methods. *arXiv preprint arXiv:2202.08545*, 2022.
- 549 Mikolaj Bińkowski, Danica J Sutherland, Michael Arbel, and Arthur Gretton. Demystifying mmd
550 gans. *arXiv preprint arXiv:1801.01401*, 2018.
- 551 Ali Borji. Pros and cons of gan evaluation measures: New developments. *Computer Vision and*
552 *Image Understanding*, 215:103329, 2022. ISSN 1077-3142.
- 553 João Carreira and Andrew Zisserman. Quo vadis, action recognition? a new model and the kinetics
554 dataset. In *2017 IEEE Conference on Computer Vision and Pattern Recognition (CVPR)*, pp.
555 4724–4733, 2017.
- 556 Haoxin Chen, Menghan Xia, Yingqing He, Yong Zhang, Xiaodong Cun, Shaoshu Yang, Jinbo Xing,
557 Yaofang Liu, Qifeng Chen, Xintao Wang, Chao Weng, and Ying Shan. Videocrafter1: Open
558 diffusion models for high-quality video generation, 2023a.
- 559 Junsong Chen, Jincheng Yu, Chongjian Ge, Lewei Yao, Enze Xie, Yue Wu, Zhongdao Wang, James
560 Kwok, Ping Luo, Huchuan Lu, and Zhenguo Li. Pixart- α : Fast training of diffusion transformer
561 for photorealistic text-to-image synthesis, 2023b.
- 562 Junsong Chen, Chongjian Ge, Enze Xie, Yue Wu, Lewei Yao, Xiaozhe Ren, Zhong-
563 dao Wang, Ping Luo, Huchuan Lu, and Zhenguo Li. Pixart- σ : *Weak – to –*
564 *strongtrainingofdiffusiontransformerfor4ktext – to – imagegeneration*, 2024a. URL.
- 565 Junsong Chen, Yue Wu, Simian Luo, Enze Xie, Sayak Paul, Ping Luo, Hang Zhao, and Zhenguo Li.
566 Pixart- δ : *Fastandcontrollableimagegenerationwithlatentconsistencymodels*, 2024b.
- 567 J. Deng, W. Dong, R. Socher, L.-J. Li, K. Li, and L. Fei-Fei. ImageNet: A Large-Scale Hierarchical
568 Image Database. In *CVPR09*, 2009.
- 569 Dan Friedman and Adji Bousso Dieng. The vendi score: A diversity evaluation metric for machine
570 learning. *Transactions on machine learning research*, 2023.
- 571 Luis Gonzalo Sanchez Giraldo, Murali Rao, and Jose C Principe. Measures of entropy from data
572 using infinitely divisible kernels. *IEEE Transactions on Information Theory*, 61(1):535–548, 2014.
- 573 Jiyeon Han, Hwanil Choi, Yunjey Choi, Junho Kim, Jung-Woo Ha, and Jaesik Choi. Rarity score :
574 A new metric to evaluate the uncommonness of synthesized images. In *The Eleventh International*
575 *Conference on Learning Representations*, 2023. URL [https://openreview.net/forum?](https://openreview.net/forum?id=JTGimap_-F)
576 [id=JTGimap_-F](https://openreview.net/forum?id=JTGimap_-F).
- 577 Jack Hessel, Ari Holtzman, Maxwell Forbes, Ronan Le Bras, and Yejin Choi. CLIPScore: a
578 reference-free evaluation metric for image captioning. In *EMNLP*, 2021.
- 579 Martin Heusel, Hubert Ramsauer, Thomas Unterthiner, Bernhard Nessler, and Sepp Hochreiter.
580 Gans trained by a two time-scale update rule converge to a local nash equilibrium. *Advances in*
581 *neural information processing systems*, 30, 2017.
- 582 Ziqi Huang, Yanan He, Jiashuo Yu, Fan Zhang, Chenyang Si, Yuming Jiang, Yuanhan Zhang, Tianx-
583 ing Wu, Qingyang Jin, Nattapol Chanpaisit, Yaohui Wang, Xinyuan Chen, Limin Wang, Dahua Lin,
584 Yu Qiao, and Ziwei Liu. VBench: Comprehensive benchmark suite for video generative models. In
585 *Proceedings of the IEEE/CVF Conference on Computer Vision and Pattern Recognition*, 2024.

- 594 Mohammad Jalali, Cheuk Ting Li, and Farzan Farnia. An information-theoretic evaluation of generative models in learning multi-modal distributions. In *Thirty-seventh Conference on Neural Information Processing Systems*, 2023.
- 595
596
597
- 598 Marco Jiralerspong, Joey Bose, Ian Gemp, Chongli Qin, Yoram Bachrach, and Gauthier Gidel. Feature likelihood score: Evaluating the generalization of generative models using samples. In *Thirty-seventh Conference on Neural Information Processing Systems*, 2023. URL <https://openreview.net/forum?id=l2VKZkolT7>.
- 600
601
- 602 Minguk Kang, Jun-Yan Zhu, Richard Zhang, Jaesik Park, Eli Shechtman, Sylvain Paris, and Taesung Park. Scaling up gans for text-to-image synthesis. In *Proceedings of the IEEE Conference on Computer Vision and Pattern Recognition (CVPR)*, 2023.
- 603
604
605
- 606 Nithish Kannan, Arif Ahmad, Marco Andreetto, Vinodkumar Prabhakaran, Utsav Prabhu, Adji Bousso Dieng, Pushpak Bhattacharyya, and Shachi Dave. Beyond aesthetics: Cultural competence in text-to-image models, 2024. URL <https://arxiv.org/abs/2407.06863>.
- 607
608
- 609 Jin-Hwa Kim, Yunji Kim, Jiyoung Lee, Kang Min Yoo, and Sang-Woo Lee. Mutual information divergence: A unified metric for multimodal generative models. In Alice H. Oh, Alekh Agarwal, Danielle Belgrave, and Kyunghyun Cho (eds.), *Advances in Neural Information Processing Systems*, 2022. URL <https://openreview.net/forum?id=wKd2XtSRsjl>.
- 610
611
612
- 613 Pum Jun Kim, Seojun Kim, and Jaejun Yoo. STREAM: Spatio-temporal evaluation and analysis metric for video generative models. In *The Twelfth International Conference on Learning Representations*, 2024. URL <https://openreview.net/forum?id=7JfKCZQPxJ>.
- 614
615
616
- 617 Tuomas Kynkäänniemi, Tero Karras, Samuli Laine, Jaakko Lehtinen, and Timo Aila. Improved precision and recall metric for assessing generative models. *Advances in Neural Information Processing Systems*, 32, 2019.
- 618
619
- 620 Tuomas Kynkäänniemi, Tero Karras, Miika Aittala, Timo Aila, and Jaakko Lehtinen. The role of imagenet classes in fréchet inception distance. In *The Eleventh International Conference on Learning Representations*, 2023. URL https://openreview.net/forum?id=4oXTQ6m_ws8.
- 621
622
623
624
- 625 Black Forest Lab. Flux: A diffusion-based text-to-image (t2i) model. <https://github.com/blackforestlab/flux>, 2024. Accessed: 2024-09.
- 626
627
- 628 Tony Lee, Michihiro Yasunaga, Chenlin Meng, Yifan Mai, Joon Sung Park, Agrim Gupta, Yunzhi Zhang, Deepak Narayanan, Hannah Benita Teufel, Marco Bellagente, Minguk Kang, Taesung Park, Jure Leskovec, Jun-Yan Zhu, Li Fei-Fei, Jiajun Wu, Stefano Ermon, and Percy Liang. Holistic evaluation of text-to-image models. In *Thirty-seventh Conference on Neural Information Processing Systems Datasets and Benchmarks Track*, 2023. URL <https://openreview.net/forum?id=qY9LR74O3Z>.
- 629
630
631
632
633
- 634 Junnan Li, Dongxu Li, Caiming Xiong, and Steven Hoi. Blip: Bootstrapping language-image pre-training for unified vision-language understanding and generation. In *ICML*, 2022.
- 635
636
- 637 Muhammad Ferjad Naeem, Seong Joon Oh, Youngjung Uh, Yunjey Choi, and Jaejun Yoo. Reliable fidelity and diversity metrics for generative models. In *International Conference on Machine Learning*, pp. 7176–7185. PMLR, 2020.
- 638
639
- 640 OpenAI. GPT-4o mini: advancing cost-efficient intelligence, July 2024.
- 641
- 642 Maxime Oquab, Timothée Darcet, Theo Moutakanni, Huy V. Vo, Marc Szafraniec, Vasil Khalidov, Pierre Fernandez, Daniel Haziza, Francisco Massa, Alaaeldin El-Nouby, Russell Howes, Po-Yao Huang, Hu Xu, Vasu Sharma, Shang-Wen Li, Wojciech Galuba, Mike Rabbat, Mido Assran, Nicolas Ballas, Gabriel Synnaeve, Ishan Misra, Herve Jegou, Julien Mairal, Patrick Labatut, Armand Joulin, and Piotr Bojanowski. Dinov2: Learning robust visual features without supervision, 2023.
- 643
644
645
646
- 647 Azim Osmanov, Jingwei Zhang, Mohammad Jalali, Xuenan Cao, Andrej Bogdanov, and Farzan Farnia. Towards a scalable reference-free evaluation of generative models. In *The Thirty-*

- 648 *eighth Annual Conference on Neural Information Processing Systems*, 2024. URL <https://openreview.net/forum?id=Ex3rPvEct8>.
- 649
- 650
- 651 Amey Pasarkar and Adji Bousso Dieng. Cousins of the vendi score: A family of similarity-based
652 diversity metrics for science and machine learning. In *International Conference on Artificial Intel-*
653 *ligence and Statistics*. PMLR, 2024.
- 654
- 655 Dustin Podell, Zion English, Kyle Lacey, Andreas Blattmann, Tim Dockhorn, Jonas Müller, Joe
656 Penna, and Robin Rombach. SDXL: Improving latent diffusion models for high-resolution image
657 synthesis. In *The Twelfth International Conference on Learning Representations*, 2024. URL
<https://openreview.net/forum?id=di52zR8xgf>.
- 658
- 659 Alec Radford, Jong Wook Kim, Chris Hallacy, Aditya Ramesh, Gabriel Goh, Sandhini Agarwal,
660 Girish Sastry, Amanda Askell, Pamela Mishkin, Jack Clark, Gretchen Krueger, and Ilya Sutskever.
661 Learning transferable visual models from natural language supervision, 2021.
- 662
- 663 Anton Razzhigaev, Arseniy Shakhmatov, Anastasia Maltseva, Vladimir Arkhipkin, Igor Pavlov, Ilya
664 Ryabov, Angelina Kuts, Alexander Panchenko, Andrey Kuznetsov, and Denis Dimitrov. Kandinsky:
665 an improved text-to-image synthesis with image prior and latent diffusion, 2023. URL <https://arxiv.org/abs/2310.03502>.
- 666
- 667 Robin Rombach, Andreas Blattmann, Dominik Lorenz, Patrick Esser, and Björn Ommer. High-
668 resolution image synthesis with latent diffusion models. In *Proceedings of the IEEE/CVF Confer-*
669 *ence on Computer Vision and Pattern Recognition (CVPR)*, pp. 10684–10695, June 2022.
- 670
- 671 Masaki Saito, Shunta Saito, Masanori Koyama, and Sosuke Kobayashi. Train sparsely, generate
672 densely: Memory-efficient unsupervised training of high-resolution temporal gan. *International*
673 *Journal of Computer Vision*, 128(10):2586–2606, Nov 2020. ISSN 1573-1405. 10.1007/s11263-
020-01333-y. URL <https://doi.org/10.1007/s11263-020-01333-y>.
- 674
- 675 Mehdi SM Sajjadi, Olivier Bachem, Mario Lucic, Olivier Bousquet, and Sylvain Gelly. Assessing
676 generative models via precision and recall. *Advances in neural information processing systems*, 31,
2018.
- 677
- 678 Tim Salimans, Ian Goodfellow, Wojciech Zaremba, Vicki Cheung, Alec Radford, Xi Chen, and
679 Xi Chen. Improved techniques for training GANs. In D. Lee, M. Sugiyama, U. Luxburg, I. Guyon,
680 and R. Garnett (eds.), *Advances in Neural Information Processing Systems*, volume 29. Curran
681 Associates, Inc., 2016.
- 682
- 683 Konstantin Shmelkov, Cordelia Schmid, and Karteek Alahari. How good is my gan? In *Proceedings*
684 *of the European conference on computer vision (ECCV)*, pp. 213–229, 2018.
- 685
- 686 George Stein, Jesse C. Cresswell, Rasa Hosseinzadeh, Yi Sui, Brendan Leigh Ross, Valentin Ville-
687 croze, Zhaoyan Liu, Anthony L. Caterini, J. Eric T. Taylor, and Gabriel Loaiza-Ganem. Exposing
flaws of generative model evaluation metrics and their unfair treatment of diffusion models, 2023.
- 688
- 689 Gemini Team. Gemini 1.5: Unlocking multimodal understanding across millions of tokens of
context, 2024. URL <https://arxiv.org/abs/2403.05530>.
- 690
- 691 Thomas Unterthiner, Sjoerd van Steenkiste, Karol Kurach, Raphaël Marinier, Marcin Michalski, and
692 Sylvain Gelly. FVD: A new metric for video generation, 2019. URL <https://openreview.net/forum?id=rylgEULtdN>.
- 693
- 694 Jianfeng Wang, Zhengyuan Yang, Xiaowei Hu, Linjie Li, Kevin Lin, Zhe Gan, Zicheng Liu, Ce Liu,
695 and Lijuan Wang. Git: A generative image-to-text transformer for vision and language, 2022. URL
696 <https://arxiv.org/abs/2205.14100>.
- 697
- 698 David Junhao Zhang, Jay Zhangjie Wu, Jia-Wei Liu, Rui Zhao, Lingmin Ran, Yuchao Gu, Difei
699 Gao, and Mike Zheng Shou. Show-1: Marrying pixel and latent diffusion models for text-to-video
generation. *arXiv preprint arXiv:2309.15818*, 2023.
- 700
- 701 Jingwei Zhang, Cheuk Ting Li, and Farzan Farnia. An interpretable evaluation of entropy-based
novelty of generative models. In Ruslan Salakhutdinov, Zico Kolter, Katherine Heller, Adrian

Weller, Nuria Oliver, Jonathan Scarlett, and Felix Berkenkamp (eds.), *Proceedings of the 41st International Conference on Machine Learning*, volume 235 of *Proceedings of Machine Learning Research*, pp. 59148–59172. PMLR, 21–27 Jul 2024. URL <https://proceedings.mlr.press/v235/zhang24ac.html>.

Zangwei Zheng, Xiangyu Peng, Tianji Yang, Chenhui Shen, Shenggui Li, Hongxin Liu, Yukun Zhou, Tianyi Li, and Yang You. Open-sora: Democratizing efficient video production for all, March 2024. URL <https://github.com/hpcaitech/Open-Sora>.

A PROOFS

A.1 PROOF OF PROPOSITION 1

First, we observe that for every $x, x' \in \mathcal{X}$ and $t, t' \in \mathcal{T}$, the following holds:

$$\begin{aligned}\phi_{X,T}([x, t])^\top \phi_{X,T}([x', t']) &= (\phi_X(x) \otimes \phi_T(t))^\top (\phi_X(x') \otimes \phi_T(t')) \\ &= (\phi_X(x)^\top \phi_X(x')) \otimes (\phi_T(t)^\top \phi_T(t')) \\ &= k_X(x, x') \otimes k_T(t, t') \\ &= k_X(x, x') k_T(t, t')\end{aligned}$$

Therefore, the Hadamard product of kernel matrices $\frac{1}{n}K_X \odot K_T$ can be written as

$$\frac{1}{n}K_X \odot K_T = \frac{1}{n}\Phi_{X,T}\Phi_{X,T}^\top$$

in terms of the matrix of samples' feature maps $\Phi_{X,T} \in \mathbb{R}^{n \times d_x d_t}$ with its i th row being $\phi_{X,T}([x_i, t_i])$. We observe that the matrices $\frac{1}{n}\Phi_{X,T}\Phi_{X,T}^\top$ and $\frac{1}{n}\Phi_{X,T}^\top\Phi_{X,T}$ share the same non-zero eigenvalues, that are the square of the singular values of $\Phi_{X,T}$. Therefore, $\frac{1}{n}K_X \odot K_T$ has the same non-zero eigenvalues as the following matrix

$$\frac{1}{n}\Phi_{X,T}^\top\Phi_{X,T} = \frac{1}{n}\sum_{i=1}^n \phi_{X,T}([x_i, t_i])\phi_{X,T}([x_i, t_i])^\top$$

which is the defined matrix $\widehat{C}_{X,T}$. Therefore, the proof of the proposition is complete.

A.2 PROOF OF COROLLARY 1

As we showed in Proposition 1, the Hadamard product $\frac{1}{n}K_X \odot K_T$ shares the same non-zero eigenvalues with $\widehat{C}_{X,T}$. Also, as noted by Jalali et al. (2023), $\frac{1}{n}K_X$ and $\frac{1}{n}K_T$ have the same non-zero eigenvalues as of \widehat{C}_X and \widehat{C}_T , respectively. Since the order- α matrix-based entropy is only a function of the input matrix's non-zero eigenvalues (zero eigenvalues have no impact on the entropy value), we can conclude that

$$\begin{aligned}H_\alpha(X|T) &:= H_\alpha\left(\frac{1}{n}K_X \odot K_T\right) - H_\alpha\left(\frac{1}{n}K_T\right) \\ &= H_\alpha(\widehat{C}_{X,T}) - H_\alpha(\widehat{C}_T),\end{aligned}$$

and also

$$\begin{aligned}I_\alpha(X; T) &:= H_\alpha\left(\frac{1}{n}K_X\right) + H_\alpha\left(\frac{1}{n}K_T\right) - H_\alpha\left(\frac{1}{n}K_X \odot K_T\right) \\ &= H_\alpha(\widehat{C}_X) + H_\alpha(\widehat{C}_T) - H_\alpha(\widehat{C}_{X,T}).\end{aligned}$$

A.3 PROOF OF THEOREM 1

To prove Theorem 1, we begin by showing the following lemma.

Lemma 1. *Suppose that the kernel function k and variable T satisfy the assumptions in Theorem 1. Then, the following Frobenius norm bound holds for $C_i = \mathbb{E}[\phi_X(x)\phi_X(x)^\top | G = i]$ where $G \in \{1, \dots, m\}$ is the cluster random variable for text T :*

$$\left\| C_{X \otimes T} - \sum_{i=1}^m \omega_i C_i \otimes \phi_T(\mu_i) \phi_T(\mu_i)^\top \right\|_F^2 \leq \frac{\sum_{i=1}^m 2\omega_i \sigma_i^2}{\sigma^2}.$$

Proof. To show this lemma, we define T_i as a variable distributed as $P_{T|G=i}$. Then,

$$\begin{aligned} & \left\| C_{X \otimes T} - \sum_{i=1}^m \omega_i C_i \otimes \phi(\mu_i) \phi(\mu_i)^\top \right\|_F^2 \\ &= \left\| \mathbb{E}[\phi_X(x)\phi_X(x)^\top \otimes \phi_T(t)\phi_T(t)^\top] - \sum_{i=1}^m \omega_i C_i \otimes \phi(\mu_i) \phi(\mu_i)^\top \right\|_F^2 \\ &= \left\| \sum_{i=1}^m \omega_i \mathbb{E}[\phi_X(x)\phi_X(x)^\top \otimes \phi_T(t)\phi_T(t)^\top | G = i] - \sum_{i=1}^m \omega_i C_i \otimes \phi(\mu_i) \phi(\mu_i)^\top \right\|_F^2 \\ &= \left\| \sum_{i=1}^m \omega_i \mathbb{E}[\phi_X(x)\phi_X(x)^\top \otimes \phi_T(t)\phi_T(t)^\top | G = i] - \sum_{i=1}^m \omega_i \mathbb{E}[\phi_X(x)\phi_X(x)^\top \otimes \phi_T(\mu_i)\phi_T(\mu_i)^\top | G = i] \right\|_F^2 \\ &= \left\| \sum_{i=1}^m \omega_i \mathbb{E}[\phi_X(x)\phi_X(x)^\top \otimes (\phi_T(t)\phi_T(t)^\top - \phi_T(\mu_i)\phi_T(\mu_i)^\top) | G = i] \right\|_F^2 \\ &\stackrel{(a)}{\leq} \sum_{i=1}^m \omega_i \mathbb{E} \left[\left\| \phi_X(x)\phi_X(x)^\top \otimes (\phi_T(t)\phi_T(t)^\top - \phi_T(\mu_i)\phi_T(\mu_i)^\top) \right\|_F^2 | G = i \right] \\ &\stackrel{(b)}{=} \sum_{i=1}^m \omega_i \mathbb{E} \left[\left\| \phi_X(x)\phi_X(x)^\top \right\|_F^2 \left\| \phi_T(t)\phi_T(t)^\top - \phi_T(\mu_i)\phi_T(\mu_i)^\top \right\|_F^2 | G = i \right] \\ &\stackrel{(c)}{=} \sum_{i=1}^m \omega_i \mathbb{E} \left[\left\| \phi_T(t)\phi_T(t)^\top - \phi_T(\mu_i)\phi_T(\mu_i)^\top \right\|_F^2 | G = i \right] \\ &\stackrel{(d)}{=} \sum_{i=1}^m \omega_i \mathbb{E} \left[2 - 2 \exp\left(-\frac{\|t - \mu_i\|_2^2}{\sigma^2}\right) | G = i \right] \\ &\stackrel{(e)}{\leq} \sum_{i=1}^m \omega_i \left[2 - 2 \exp\left(\frac{-\mathbb{E}[\|t - \mu_i\|_2^2 | G = i]}{\sigma^2}\right) \right] \\ &\stackrel{(f)}{\leq} \sum_{i=1}^m \omega_i \left[2 - 2 \exp\left(\frac{-\sigma_i^2}{\sigma^2}\right) \right] \\ &\stackrel{(g)}{\leq} \sum_{i=1}^m 2\omega_i \frac{\sigma_i^2}{\sigma^2} \end{aligned}$$

In the above, (a) follows from Jensen's inequality for the convex Frobenius-norm-squared function. (b) holds because $\|A \otimes B\|_F^2 = \|A\|_F^2 \|B\|_F^2$ for every matrices A, B . (c) comes from the normalized Gaussian kernel satisfying $\langle \phi_T(t), \phi_T(t) \rangle = k(t, t) = 1$, resulting in $\|\phi_T(t)\phi_T(t)^\top\|_F^2 = \text{Tr}(\phi_T(t)\phi_T(t)^\top \phi_T(t)\phi_T(t)^\top) = \text{Tr}(\phi_T(t)\phi_T(t)^\top) = 1$. (d) follows from the Gaussian kernel definition, proving that $\phi_T(t)^\top \phi_T(\mu_i) = \exp(-\|t - \mu_i\|_2^2 / 2\sigma^2)$. (e) shows the application of Jensen's inequality to the concave $s(z) = 1 - \exp(-z)$. (f) holds because $s(z) = 1 - \exp(-z)$ is a monotonically increasing function. Finally, (g) follows from the inequality $1 - \exp(-z) \leq z$ for every scalar z . Therefore, the proof is complete. \square

Next, we apply the Gram–Schmidt process to $\phi_T(\mu_1), \dots, \phi_T(\mu_m)$ to find orthogonal vectors u_1, \dots, u_m . We let $u_1 = \phi_T(\mu_1)$. Then, for every $2 \leq i \leq m$, we define

$$u_i := \phi(\mu_i) - \sum_{j=1}^{i-1} \langle \phi(\mu_i), u_j \rangle u_j.$$

As a result, the following holds

$$\begin{aligned} & \left\| \sum_{i=1}^m \omega_i C_i \otimes \phi(\mu_i) \phi(\mu_i)^\top - \sum_{i=1}^m \omega_i C_i \otimes u_i u_i^\top \right\|_F^2 \\ &= \left\| \sum_{i=1}^m \omega_i C_i \otimes \left(\phi(\mu_i) \phi(\mu_i)^\top - u_i u_i^\top \right) \right\|_F^2 \\ &\stackrel{(h)}{\leq} \sum_{i=1}^m \omega_i \left\| C_i \otimes \left(\phi(\mu_i) \phi(\mu_i)^\top - u_i u_i^\top \right) \right\|_F^2 \\ &= \sum_{i=1}^m \omega_i \left\| C_i \right\|_F^2 \left\| \phi(\mu_i) \phi(\mu_i)^\top - u_i u_i^\top \right\|_F^2 \\ &\stackrel{(i)}{\leq} \sum_{i=1}^m \omega_i \left\| \phi(\mu_i) \phi(\mu_i)^\top - u_i u_i^\top \right\|_F^2 \\ &\stackrel{(j)}{=} \sum_{i=1}^m \omega_i \left(1 + \|u_i\|^4 - 2(u_i^\top \phi_T(\mu_i))^2 \right) \\ &\leq \sum_{i=1}^m \omega_i \left(2 - 2(u_i^\top \phi(\mu_i))^2 \right) \\ &= 2 \sum_{i=1}^m \omega_i \left(1 + u_i^\top \phi(\mu_i) \right) \left(1 - u_i^\top \phi(\mu_i) \right) \\ &\stackrel{(k)}{\leq} 4 \sum_{i=1}^m \sum_{j=1}^{i-1} \omega_i \exp\left(-\frac{\|\mu_i - \mu_j\|_2^2}{\sigma^2} \right). \end{aligned}$$

Here, (h) follows from the application of Jensen’s inequality for the convex Frobenius-norm-squared.

(i) holds since the text kernel is normalized and $\langle \phi_X(x), \phi_X(x) \rangle = k_X(x, x) = 1$, and therefore $\|C_i\|_F \leq \mathbb{E}[\|\phi_X(x)\|_2^2] = 1$. (j) follows from the expansion $\|uu^\top - vv^\top\|_F^2 = \|u\|_2^4 + \|v\|_2^4 - 2\langle u, v \rangle^2$. (k) holds because $u_i^\top \phi_T(\mu_i) \leq 1$ and

$$u_i^\top \phi_T(\mu_i) = 1 - \sum_{j=1}^{i-1} \langle \phi_T(\mu_i), u_j \rangle^2 \geq 1 - \sum_{j=1}^{i-1} \exp\left(-\frac{\|\mu_i - \mu_j\|_2^2}{\sigma^2} \right).$$

Since we know that for every matrices $A, B \in \mathbb{R}^{d \times d}$, $\|A + B\|_F^2 \leq 2\|A\|_F^2 + 2\|B\|_F^2$, the above results show that

$$\left\| C_{X \otimes T} - \sum_{i=1}^m \omega_i C_i \otimes u_i u_i^\top \right\|_F^2 \leq \sum_{i=1}^m 4\omega_i \frac{\sigma_i^2}{\sigma^2} + \sum_{i=2}^m \sum_{j=1}^{i-1} 8\omega_i \exp\left(-\frac{\|\mu_i - \mu_j\|_2^2}{\sigma^2} \right).$$

As a result, the Hoffman-Wielandt inequality shows that for the sorted eigenvalues vector λ of $C_{X \otimes T}$ and sorted eigenvalues vector $\tilde{\lambda}$ of $\sum_{i=1}^m \omega_i C_i \otimes u_i u_i^\top$ the following holds:

$$\begin{aligned} \|\lambda - \tilde{\lambda}\|_2^2 &\leq \left\| C_{X \otimes T} - \sum_{i=1}^m \omega_i C_i \otimes u_i u_i^\top \right\|_F^2 \\ &\leq \sum_{i=1}^m 4\omega_i \frac{\sigma_i^2}{\sigma^2} + \sum_{i=2}^m \sum_{j=1}^{i-1} 8\omega_i \exp\left(-\frac{\|\mu_i - \mu_j\|_2^2}{\sigma^2} \right). \end{aligned}$$

Since u_1, \dots, u_m are orthogonal vectors, the definition of Kronecker product implies that the eigenvalues of $\sum_{i=1}^m \omega_i C_i \otimes u_i u_i^\top$ will be the union of the eigenvalues of $\omega_i C_i \otimes u_i u_i^\top$ over $i \in \{1, \dots, m\}$. On the other hand, we know that the non-zero eigenvalues of $\omega_i C_i \otimes u_i u_i^\top$ will be equal to the factor $\omega_i \|u_i\|_2^2$ times the eigenvalues of C_i . Also, we know that $1 \geq \|u_i\|_2^2 \geq 1 - 2 \sum_{j=1}^{i-1} \exp(-\frac{\|\mu_i - \mu_j\|_2^2}{\sigma^2})$. Consequently, we can show that for vector $\hat{\lambda}_{x \otimes t} = \text{Union}(\omega_i \text{Eigs}(C_i) : i \in \{1, \dots, m\})$, we have the following for every $\alpha \geq 2$ and defined increasing function g in Theorem 1

$$\begin{aligned} \left| \tilde{H}_\alpha(X, T) - \frac{1}{1-\alpha} \log(\|\hat{\lambda}_{x \otimes t}\|_\alpha^\alpha) \right| &\leq g(\|\tilde{\lambda}_{x \otimes t}\|_\alpha - \|\hat{\lambda}_{x \otimes t}\|_\alpha) \\ &\leq g(\|\text{sort}(\tilde{\lambda}_{x \otimes t}) - \text{sort}(\hat{\lambda}_{x \otimes t})\|_\alpha) \\ &\leq g(\|\text{sort}(\tilde{\lambda}_{x \otimes t}) - \text{sort}(\hat{\lambda}_{x \otimes t})\|_2) \\ &\leq g\left(\sum_{i=1}^m 4\omega_i \frac{\sigma_i^2}{\sigma^2} + \sum_{i=2}^m \sum_{j=1}^{i-1} 16\omega_i \exp\left(-\frac{\|\mu_i - \mu_j\|_2^2}{\sigma^2}\right)\right). \end{aligned}$$

Note that the above proof holds for every marginal distribution on X , and we choose a deterministic constant $X = \mathbf{0}$, then the joint entropy reduces to the marginal entropy and the above inequality also shows the following:

$$\left| \tilde{H}_\alpha(T) - \frac{1}{1-\alpha} \log(\|\omega_1, \dots, \omega_m\|_\alpha^\alpha) \right| \leq g\left(\sum_{i=1}^m 4\omega_i \frac{\sigma_i^2}{\sigma^2} + \sum_{i=2}^m \sum_{j=1}^{i-1} 16\omega_i \exp\left(-\frac{\|\mu_i - \mu_j\|_2^2}{\sigma^2}\right)\right).$$

Therefore, following the Triangle inequality and the definition $\tilde{H}_\alpha(X|T) = \tilde{H}_\alpha(X, T) - \tilde{H}_\alpha(T)$, the previous two inequalities prove that

$$\begin{aligned} &\left| \tilde{H}_\alpha(X|T) - \left(\frac{1}{1-\alpha} \log(\|\hat{\lambda}_{x \otimes t}\|_\alpha^\alpha) - \frac{1}{1-\alpha} \log(\|\omega_1, \dots, \omega_m\|_\alpha^\alpha) \right) \right| \\ &\leq 2g\left(\sum_{i=1}^m 4\omega_i \frac{\sigma_i^2}{\sigma^2} + \sum_{i=2}^m \sum_{j=1}^{i-1} 16\omega_i \exp\left(-\frac{\|\mu_i - \mu_j\|_2^2}{\sigma^2}\right)\right). \end{aligned}$$

On the other hand, we can simplify the above expression as

$$\begin{aligned} &\frac{1}{1-\alpha} \log(\|\hat{\lambda}_{x \otimes t}\|_\alpha^\alpha) - \frac{1}{1-\alpha} \log(\|\omega_1, \dots, \omega_m\|_\alpha^\alpha) \\ &= \frac{1}{1-\alpha} \log\left(\sum_{i=1}^m \omega_i^\alpha \|\lambda_{C_i}\|_\alpha^\alpha\right) - \frac{1}{1-\alpha} \log\left(\sum_{i=1}^m \omega_i^\alpha\right) \\ &= \frac{1}{1-\alpha} \log\left(\sum_{i=1}^m \frac{\omega_i^\alpha}{\sum_{j=1}^m \omega_j^\alpha} \|\lambda_{C_i}\|_\alpha^\alpha\right) \end{aligned}$$

Note that the definition $f_\alpha(t) = \exp((1-\alpha)t)$ implies that $f_\alpha^{-1}(z) = \frac{1}{1-\alpha} \log(z)$, which connects to the entropy definition as $H(X|G=i) = f_\alpha^{-1}(\|\lambda_{C_i}\|_\alpha^\alpha)$. As a result, we can combine the previous two equations and complete the proof as:

$$\begin{aligned} &\left| \tilde{H}_\alpha(X|T) - f_\alpha^{-1}\left(\sum_{i=1}^m \frac{\omega_i^\alpha}{\sum_{j=1}^m \omega_j^\alpha} f_\alpha(\tilde{H}_\alpha(X|G=i))\right) \right| \\ &\leq 2g\left(\sum_{i=1}^m 4\omega_i \frac{\sigma_i^2}{\sigma^2} + \sum_{i=2}^m \sum_{j=1}^{i-1} 16\omega_i \exp\left(-\frac{\|\mu_i - \mu_j\|_2^2}{\sigma^2}\right)\right). \end{aligned}$$



Figure 8: Substituting images generated from models trained on MS-COCO dataset.

B ADDITIONAL NUMERICAL RESULTS

B.1 CORRELATION BETWEEN PROMPTS AND GENERATED OUTPUT

To measure the correlation between text and image using Information-Vendi, we used MS-COCO captions to generate images with Stable Diffusion XL and Flux. We gradually substituted the generated images with random ones for the same prompts at different substitution rates. As the substitution rate increased, the correlation between the text and image pairs decreased. In Figure 8, we measured Information-Vendi at various substitution rates and observed that as the substitution rate increased, Information-Vendi decreased, demonstrating that our score can successfully measure the correlation between text and image. Unlike other correlation metrics, such as CLIPScore, which require the same embedding for both text and image, our method places no such restriction. This allows for the use of different embeddings for text and image. Furthermore, our approach can be easily generalized to other conditional models, such as text-to-text or text-to-video generation.

B.2 MEASURING CONDITIONAL-VENDI ACROSS PROMPT TYPES

In this section, we conducted additional experiments similar to those in Figure 5. We created 5,000 prompts across different categories using GPT4o and generated corresponding images with text-to-image models. We reported Conditional-Vendi for the top 3 groups in the text data on PixArt- α , Stable Diffusion XL text-to-image generative models.

As shown in Figure 9, Figure 10 and Figure 11, we observed the same behavior during these experiments: the Conditional-Vendi score for "dog" prompts was significantly higher than for the "airplane" and "sofa" categories. This observation suggests that the outputs of generative models are unbalanced when presented with different groups of text prompts.

B.3 QUANTIFYING MODEL-INDUCED DIVERSITY VIA CONDITIONAL-VENDI.

In this section, we provided a more detailed version of Figure 3. As shown in Figure 12, we found that Conditional-Vendi increased at a more rapid rate when the prompts did not specify the type of animal in the picture. In contrast, when the animal types were specified in the prompts, there was only a slight increase in the Conditional-Vendi score.

B.4 ADDITIONAL NUMERICAL EVALUATION OF THE CONDITIONAL-VENDI SCORE

To further experiment the correlation between the intrinsic model diversity and the defined Conditional-Vendi score, we have performed experiments of quantifying the diversity scores for unspecified and type-specified prompts when generating data from standard text-to-image models. To conduct an extensive evaluation of the Conditional-Vendi score, we performed the experiments on the nine combinations of three category types, 1) animals, 2) fruits, 3) objects, and three SOTA text-to-image generation models SDXL, Kandinsky, and PixArt- Σ Chen et al. (2024a). In each

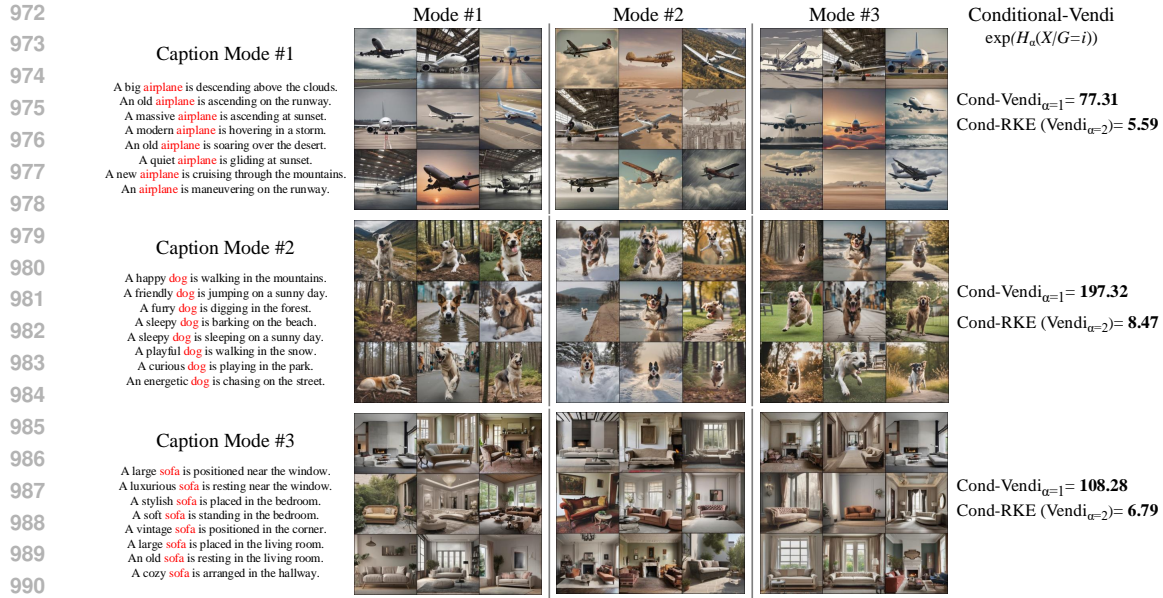


Figure 9: Quantifying image diversity for different clusters of text prompts. Images are generated using the Stable Diffusion XL model.



Figure 10: Quantifying image diversity for different clusters of text prompts. Images are generated using the PixArt- α model.

of the nine experiments, we generated prompts on 10 different types related to each category and created image samples by inputting the prompts to the text-to-image model. In each experiment, we simulated 10 prompt-based generative models by considering image samples from j types for $j \in \{1, \dots, 10\}$.

In addition, given the original prompts specifying the type of category in the image, we compared the Vendi and Conditional-Vendi scores among the three text-to-image models. Figures ??? show the comparison between the scores of the three models, which suggest the higher intrinsic diversity measure by Conditional-Vendi for the SD-XL and PixArt- Σ models.

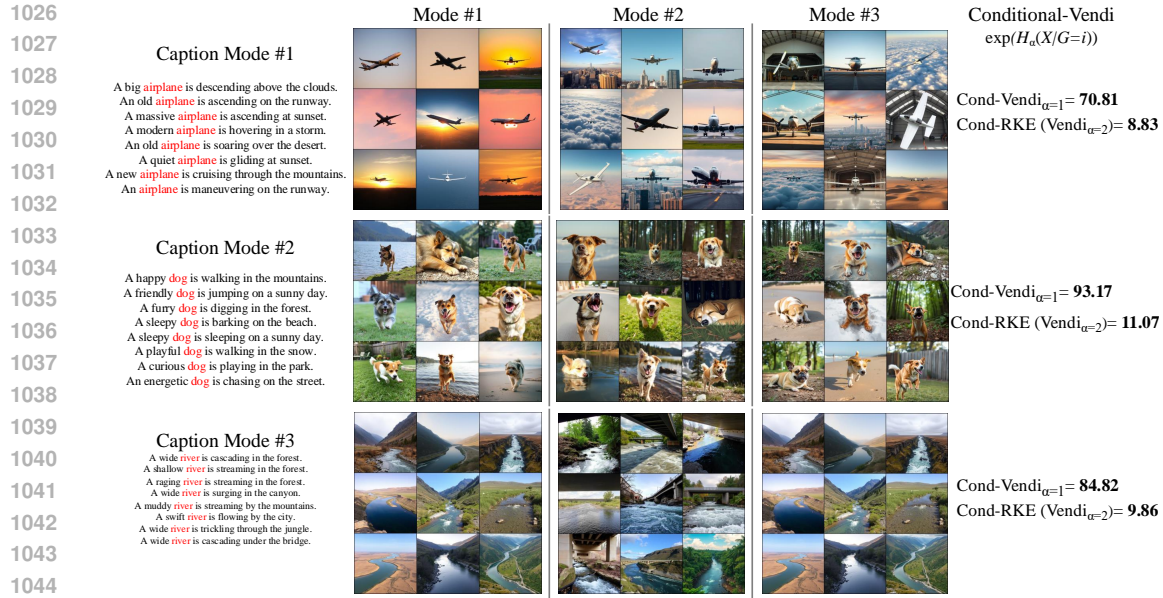


Figure 11: Quantifying image diversity for different clusters of text prompts. Images are generated using the Flux model.

B.5 CORRELATION BETWEEN GROUNDTRUTH-CLUSTER-VENDI AND CONDITIONAL-VENDI SCORES

To validate the theoretical connection between the Vendi and Conditional-Vendi scores, we performed an experiment and evaluated a baseline metric called GroundTruth-Cluster-Vendi score. To measure the GroundTruth-Cluster-Vendi score, we utilize the side knowledge of the ground-truth clusters of the input prompts and then compute and average the regular Vendi scores for the data generated within each cluster. Mathematically, given t sample cluster sets in $\mathcal{S} = \{S_1, \dots, S_t\}$, which partition the input text indices $\{1, \dots, n\}$, we define the Cluster-Vendi score as follows, where $|S_j|$ denotes the cardinality of subset S_j :

$$\text{Cluster-Vendi}(x_1, \dots, x_n | \mathcal{S}) := \sum_{i=1}^t \frac{|S_i|}{n} \cdot \text{Vendi}(\{x_j : j \in S_i\}).$$

Note that the above definition requires the knowledge of the clusters, which could be given by an oracle in the case of the GroundTruth-Cluster-Vendi score, or computed by a clustering algorithm such as K-Means to obtain the KMeans-Cluster-Vendi score. Observe that given the knowledge of the clusters revealed by an oracle, the GroundTruth-Cluster-Vendi score is a sensible definition of internal model diversity, which, as shown in Theorem 1, is expected to correlate with our defined Conditional-Vendi score.

In the numerical settings of the previous section, where we know the ground-truth clusters based on the type of animal, fruit, or object in the texts, we computed the value of the GroundTruth-Cluster-Vendi score and compared it with the evaluated Conditional-Vendi score. As demonstrated in Figures 22, the two diversity scores, Conditional-Vendi and GroundTruth-Cluster-Vendi, highly correlate for the ten simulated generative models in the experiments.

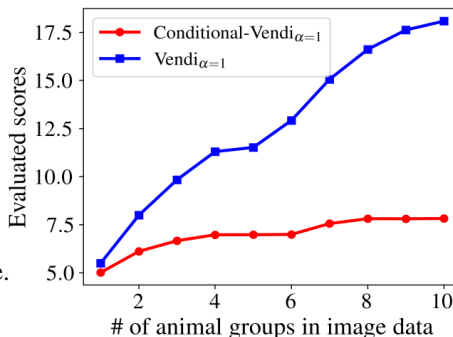
However, note that in a real-world scenario, we do not have access to the ground-truth clusters. To estimate the score, we should use a clustering algorithm such as K-Means to find the clusters and compute the Cluster-Vendi score. We note that the optimization problem addressed by standard clustering algorithms represents a challenging non-convex optimization, which, depending on the algorithm’s initial point, could converge to different solutions. Our numerical results with the K-Means clustering algorithm in Figure 23 also demonstrated these clustering challenges and, in several cases, failed to find the ground-truth clusters with high accuracy.

1080
1081
1082
1083
1084
1085
1086
1087
1088
1089
1090
1091
1092
1093
1094
1095
1096
1097
1098
1099
1100
1101
1102
1103
1104
1105
1106
1107
1108
1109
1110
1111
1112
1113
1114
1115
1116
1117
1118
1119
1120
1121
1122
1123
1124
1125
1126
1127
1128
1129
1130
1131
1132
1133

Type-specified animal prompts

Prompts:

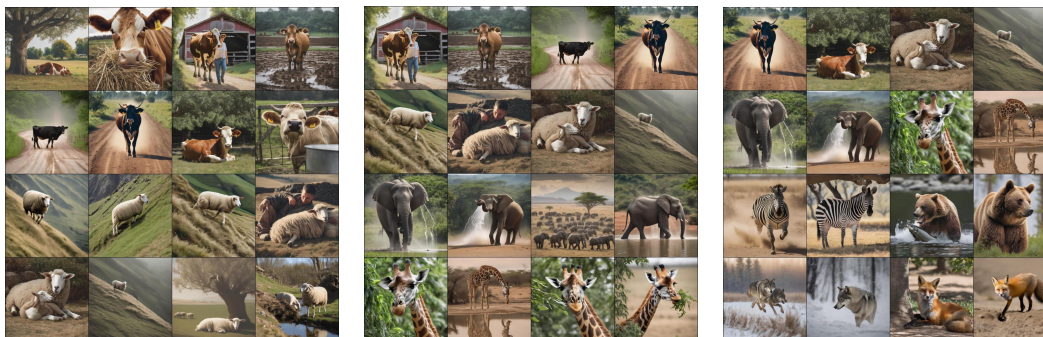
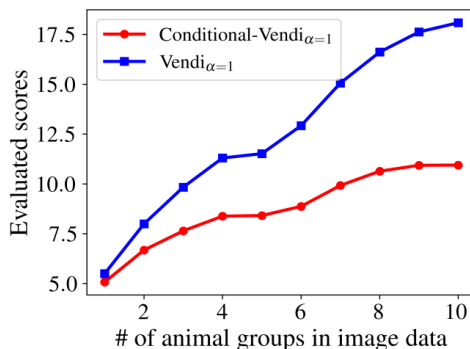
- A fox is rolling in the grass.
- A camel is resting near a sand dune.
- A wolf is drinking from a river.
- A cow is resting under a tree.
- A sheep is resting in a grassy pasture.
- An elephant is walking through thick jungle.
- A giraffe is reaching up for leaves.



Unspecified animal prompts

Prompts:

- An animal is rolling in the grass.
- An animal resting near a sand dune.
- An animal is drinking from a river.
- An animal is resting under a tree.
- An animal is resting in a grassy pasture.
- An animal is walking through jungle.
- An animal is reaching up for leaves.



Model 2: Samples from 2 animal groups Model 4: Samples from 4 animal groups Model 8: Samples from 8 animal groups

Figure 12: Comparing Conditional-Vendi with Vendi on different animal groups generated by Stable Diffusion-XL.

B.6 ALGORITHM FOR COMPUTING CONDITIONAL-VENDI AND INFORMATION-VENDI

In this section, we present the algorithm to compute the Conditional-Vendi and Information-Vendi scores. Using the definition provided in Section 4, combined with the entropy definition in equation 3, we calculate the Conditional-Vendi score. The steps are outlined in Algorithm 1.

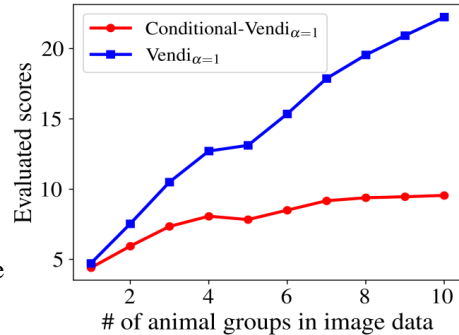
B.7 QUALITATIVE RESULTS FOR GENERATIVE MODELS TRAINED ON MS-COCO DATASET

In this section, we provide images and prompts corresponding to Figure 4. Figure 25 illustrates three clusters obtained by applying KMeans to cluster MS-COCO validation set prompts into 1000 clusters. The images are presented for four generative models. Comparing the prompts with the generated images reveals that FLUX exhibits the highest alignment between text and image, while

Type-specified animal prompts

Prompts:

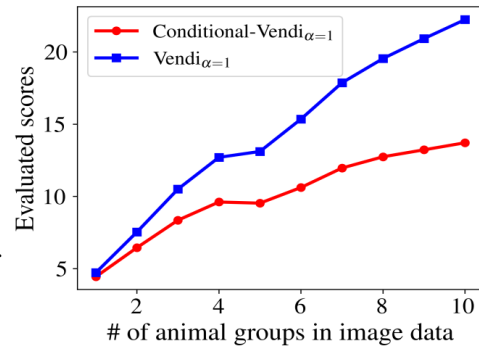
A **fox** is rolling in the grass.
 A **camel** is resting near a sand dune.
 A **wolf** is drinking from a river.
 A **cow** is resting under a tree.
 A **sheep** is resting in a grassy pasture.
 An **elephant** is walking through thick jungle
 A **giraffe** is reaching up for leaves.



Unspecified animal prompts

Prompts:

An **animal** is rolling in the grass.
 An **animal** resting near a sand dune.
 An **animal** is drinking from a river.
 An **animal** is resting under a tree.
 An **animal** is resting in a grassy pasture.
 An **animal** is walking through jungle.
 An **animal** is reaching up for leaves.



Model 2:
Samples from 2 animal groups

Model 4:
Samples from 4 animal groups

Model 8:
Samples from 8 animal groups

Figure 13: Comparing Conditional-Vendi with Vendi on different animal groups generated by PixArtΣ.

GigaGAN demonstrates greater diversity but misses some features of the prompts. These observations are further supported by the Conditional-Vendi and Information-Vendi metrics.

B.8 EFFECT OF BANDWIDTH ON CONDITIONAL-VENDI AND INFORMATION-VENDI

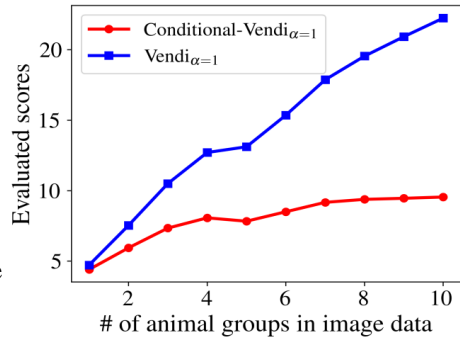
To further investigate the effect of bandwidth on Conditional-Vendi and Information-Vendi, we began by selecting the image bandwidth similar to prior works Friedman & Dieng (2023); Ospanov et al. (2024). We then measured and plotted the scores using varying text kernel bandwidths. Figure 26 demonstrates consistent rankings of the four models across different bandwidth parameters. The results indicate that as the kernel bandwidth increases, the number of text clusters increases, leading to a decrease in the Information-Vendi value.

1188
1189
1190
1191
1192
1193
1194
1195
1196
1197
1198
1199
1200
1201
1202
1203
1204
1205
1206
1207
1208
1209
1210
1211
1212
1213
1214
1215
1216
1217
1218
1219
1220
1221
1222
1223
1224
1225
1226
1227
1228
1229
1230
1231
1232
1233
1234
1235
1236
1237
1238
1239
1240
1241

Type-specified animal prompts

Prompts:

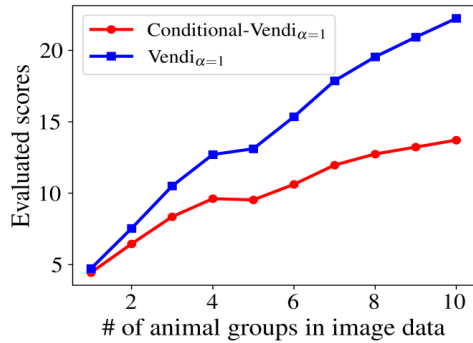
A **fox** is rolling in the grass.
 A **camel** is resting near a sand dune.
 A **wolf** is drinking from a river.
 A **cow** is resting under a tree.
 A **sheep** is resting in a grassy pasture.
 An **elephant** is walking through thick jungle
 A **giraffe** is reaching up for leaves.



Unspecified animal prompts

Prompts:

An **animal** is rolling in the grass.
 An **animal** resting near a sand dune.
 An **animal** is drinking from a river.
 An **animal** is resting under a tree.
 An **animal** is resting in a grassy pasture.
 An **animal** is walking through jungle.
 An **animal** is reaching up for leaves.



Model 2: Samples from 2 animal groups Model 4: Samples from 4 animal groups Model 8: Samples from 8 animal groups

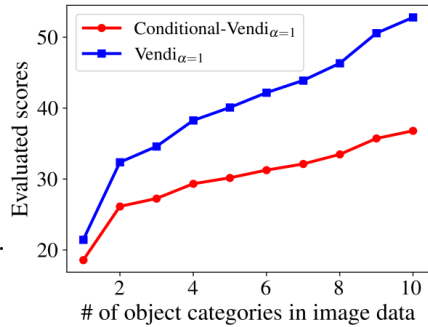
Figure 14: Comparing Conditional-Vendi with Vendi on different animal groups generated by Kandinsky.

1242
1243
1244
1245
1246
1247
1248
1249
1250
1251
1252
1253
1254
1255
1256
1257
1258
1259
1260
1261
1262
1263
1264
1265
1266
1267
1268
1269
1270
1271
1272
1273
1274
1275
1276
1277
1278
1279
1280
1281
1282
1283
1284
1285
1286
1287
1288
1289
1290
1291
1292
1293
1294
1295

Type-specified object prompts

Prompts:

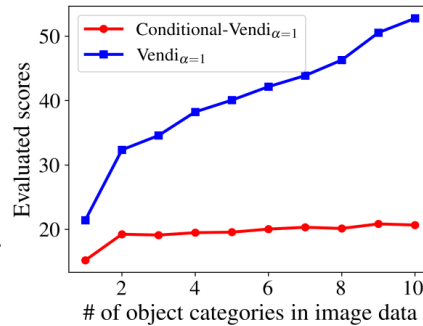
- A **Chair** is placed under a sprawling tree.
- A **Sofa** is glowing in the light of a nearby fire.
- A **Book** is balancing on the edge of a table.
- A **Clock** is positioned in an office setup.
- A **Lamp** is sitting under a hanging light bulb.
- A **laptop** is half-hidden behind a stack of boxes.
- A **car** is in the corner of a large warehouse.
- The **cup** is precariously balanced on rocks.



Unspecified object prompts

Prompts:

- An **object** is placed under a sprawling tree.
- An **object** is glowing in the light of a nearby fire.
- An **object** is balancing on the edge of a table.
- An **object** is positioned in an office setup.
- An **object** is sitting under a hanging light bulb.
- An **object** is half-hidden behind a stack of boxes.
- An **object** is in the corner of a large warehouse.
- The **object** is precariously balanced on rocks.



Model 2:
Samples from 2 fruit types

Model 4:
Samples from 4 fruit types

Model 8:
Samples from 8 fruit types

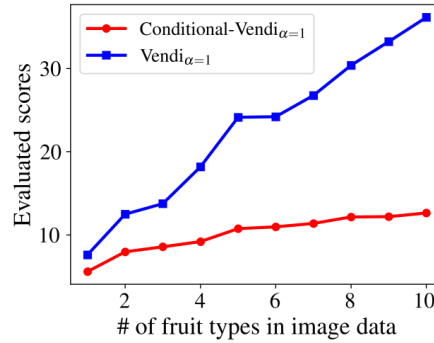
Figure 15: Comparing Conditional-Vendi with Vendi on different fruit types generated by Stable Diffusion-XL.

1296
1297
1298
1299
1300
1301
1302
1303
1304
1305
1306
1307
1308
1309
1310
1311
1312
1313
1314
1315
1316
1317
1318
1319
1320
1321
1322
1323
1324
1325
1326
1327
1328
1329
1330
1331
1332
1333
1334
1335
1336
1337
1338
1339
1340
1341
1342
1343
1344
1345
1346
1347
1348
1349

Type-specified fruit prompts

Prompts:

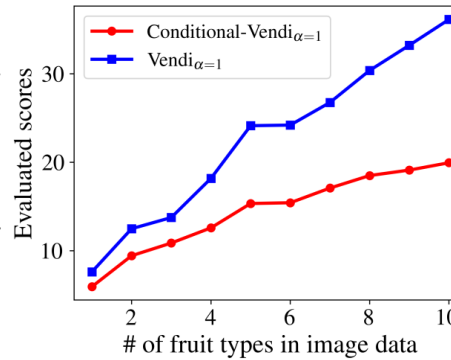
An **apple** is next to a cold glass of fresh juice.
 A **banana** is being sliced with a sharp knife.
 The **watermelon** is blended into a smoothie.
 The **pineapple** is falling out of a grocery bag.
 A **strawberry** is being washed.
 The **peach** is sitting on a kitchen countertop.
 A **cherry** is being sliced with a knife.
 A **mango** is sitting on a colorful plate.



Unspecified fruit prompts

Prompts:

A **fruit** is next to a cold glass of fresh juice.
 A **fruit** is being sliced with a sharp knife.
 The **fruit** is blended into a smoothie.
 The **fruit** is falling out of a grocery bag.
 A **fruit** is being washed.
 The **fruit** is sitting on a kitchen countertop.
 A **fruit** is being sliced with a knife.
 A **fruit** is sitting on a colorful plate.



Model 2:
Samples from 2 fruit types

Model 4:
Samples from 4 fruit types

Model 8:
Samples from 8 fruit types

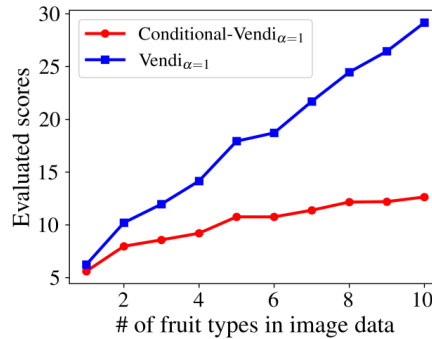
Figure 16: Comparing Conditional-Vendi with Vendi on different fruit types generated by Kandinsky.

1350
1351
1352
1353
1354
1355
1356
1357
1358
1359
1360
1361
1362
1363
1364
1365
1366
1367
1368
1369
1370
1371
1372
1373
1374
1375
1376
1377
1378
1379
1380
1381
1382
1383
1384
1385
1386
1387
1388
1389
1390
1391
1392
1393
1394
1395
1396
1397
1398
1399
1400
1401
1402
1403

Type-specified fruit prompts

Prompts:

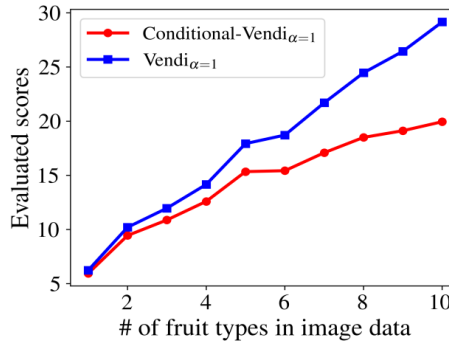
An **apple** is next to a cold glass of fresh juice.
 A **banana** is being sliced with a sharp knife.
 The **watermelon** is blended into a smoothie.
 The **pineapple** is falling out of a grocery bag.
 A **strawberry** is being washed.
 The **peach** is sitting on a kitchen countertop.
 A **cherry** is being sliced with a knife.
 A **mango** is sitting on a colorful plate.



Unspecified fruit prompts

Prompts:

A **fruit** is next to a cold glass of fresh juice.
 A **fruit** is being sliced with a sharp knife.
 The **fruit** is blended into a smoothie.
 The **fruit** is falling out of a grocery bag.
 A **fruit** is being washed.
 The **fruit** is sitting on a kitchen countertop.
 A **fruit** is being sliced with a knife.
 A **fruit** is sitting on a colorful plate.



Model 2:
Samples from 2 fruit types

Model 4:
Samples from 4 fruit types

Model 8:
Samples from 8 fruit types

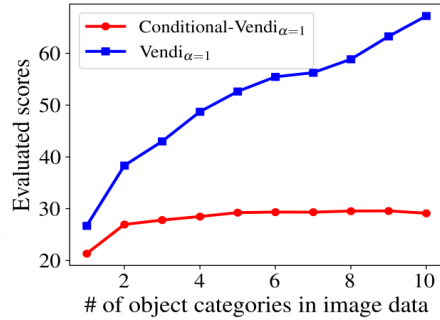
Figure 17: Comparing Conditional-Vendi with Vendi on different fruit types generated by PixArt- Σ .

1404
1405
1406
1407
1408
1409
1410
1411
1412
1413
1414
1415
1416
1417
1418
1419
1420
1421
1422
1423
1424
1425
1426
1427
1428
1429
1430
1431
1432
1433
1434
1435
1436
1437
1438
1439
1440
1441
1442
1443
1444
1445
1446
1447
1448
1449
1450
1451
1452
1453
1454
1455
1456
1457

Type-specified object prompts

Prompts:

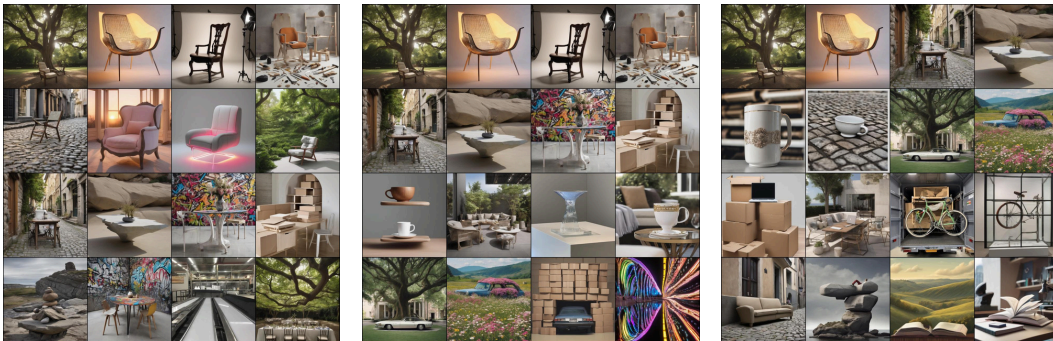
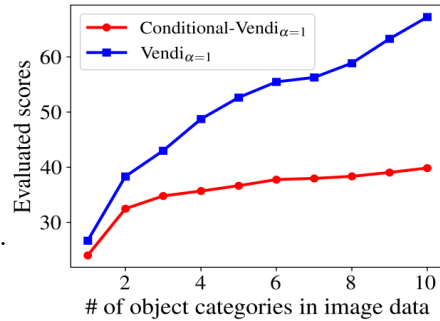
- A **Chair** is placed under a sprawling tree.
- A **Sofa** is glowing in the light of a nearby fire.
- A **Book** is balancing on the edge of a table.
- A **Clock** is positioned in an office setup.
- A **Lamp** is sitting under a hanging light bulb.
- A **laptop** is half-hidden behind a stack of boxes.
- A **car** is in the corner of a large warehouse.
- The **cup** is precariously balanced on rocks.



Unspecified object prompts

Prompts:

- An **object** is placed under a sprawling tree.
- An **object** is glowing in the light of a nearby fire.
- An **object** is balancing on the edge of a table.
- An **object** is positioned in an office setup.
- An **object** is sitting under a hanging light bulb.
- An **object** is half-hidden behind a stack of boxes.
- An **object** is in the corner of a large warehouse.
- The **object** is precariously balanced on rocks.



Model 2: Samples from 2 object categories Model 4: Samples from 4 object categories Model 8: Samples from 8 object categories

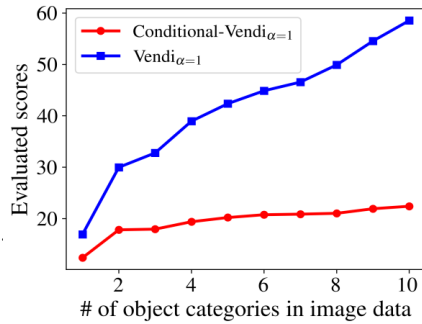
Figure 18: Comparing Conditional-Vendi with Vendi on different fruit types generated by Stable Diffusion-XL.

1458
1459
1460
1461
1462
1463
1464
1465
1466
1467
1468
1469
1470
1471
1472
1473
1474
1475
1476
1477
1478
1479
1480
1481
1482
1483
1484
1485
1486
1487
1488
1489
1490
1491
1492
1493
1494
1495
1496
1497
1498
1499
1500
1501
1502
1503
1504
1505
1506
1507
1508
1509
1510
1511

Type-specified object prompts

Prompts:

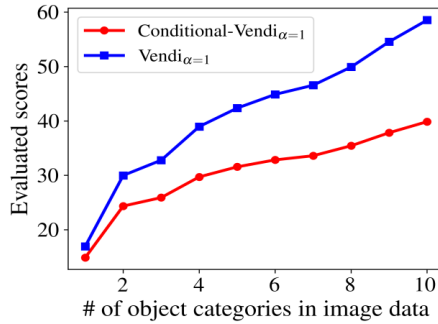
- A **Chair** is placed under a sprawling tree.
- A **Sofa** is glowing in the light of a nearby fire.
- A **Book** is balancing on the edge of a table.
- A **Clock** is positioned in an office setup.
- A **Lamp** is sitting under a hanging light bulb.
- A **laptop** is half-hidden behind a stack of boxes.
- A **car** is in the corner of a large warehouse.
- The **cup** is precariously balanced on rocks.



Unspecified object prompts

Prompts:

- An **object** is placed under a sprawling tree.
- An **object** is glowing in the light of a nearby fire.
- An **object** is balancing on the edge of a table.
- An **object** is positioned in an office setup.
- An **object** is sitting under a hanging light bulb.
- An **object** is half-hidden behind a stack of boxes.
- An **object** is in the corner of a large warehouse.
- The **object** is precariously balanced on rocks.



Model 2: Samples from 2 object categories Model 4: Samples from 4 object categories Model 8: Samples from 8 object categories

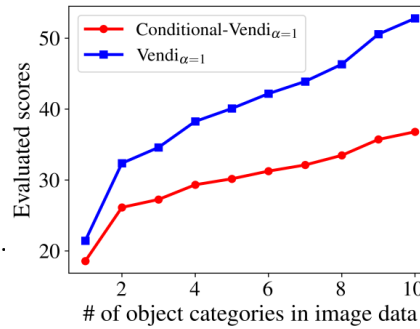
Figure 19: Comparing Conditional-Vendi with Vendi on different object categories types generated by Kandinsky.

1512
1513
1514
1515
1516
1517
1518
1519
1520
1521
1522
1523
1524
1525
1526
1527
1528
1529
1530
1531
1532
1533
1534
1535
1536
1537
1538
1539
1540
1541
1542
1543
1544
1545
1546
1547
1548
1549
1550
1551
1552
1553
1554
1555
1556
1557
1558
1559
1560
1561
1562
1563
1564
1565

Type-specified object prompts

Prompts:

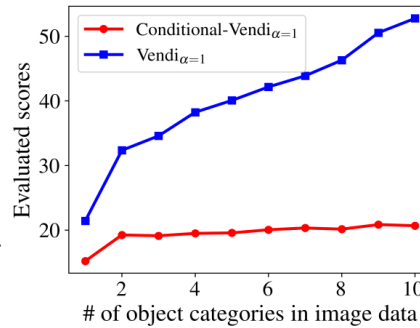
- A **Chair** is placed under a sprawling tree.
- A **Sofa** is glowing in the light of a nearby fire.
- A **Book** is balancing on the edge of a table.
- A **Clock** is positioned in an office setup.
- A **Lamp** is sitting under a hanging light bulb.
- A **laptop** is half-hidden behind a stack of boxes.
- A **car** is in the corner of a large warehouse.
- The **cup** is precariously balanced on rocks.



Unspecified object prompts

Prompts:

- An **object** is placed under a sprawling tree.
- An **object** is glowing in the light of a nearby fire.
- An **object** is balancing on the edge of a table.
- An **object** is positioned in an office setup.
- An **object** is sitting under a hanging light bulb.
- An **object** is half-hidden behind a stack of boxes.
- An **object** is in the corner of a large warehouse.
- The **object** is precariously balanced on rocks.



Model 2: Samples from 2 object categories Model 4: Samples from 4 object categories Model 8: Samples from 8 object categories

Figure 20: Comparing Conditional-Vendi with Vendi on different object categories types generated by PixArt-Σ.

1566
 1567
 1568
 1569
 1570
 1571
 1572
 1573
 1574
 1575
 1576
 1577
 1578
 1579
 1580
 1581
 1582
 1583
 1584
 1585
 1586
 1587
 1588
 1589
 1590
 1591
 1592
 1593
 1594
 1595
 1596
 1597
 1598
 1599
 1600
 1601
 1602
 1603
 1604
 1605
 1606
 1607
 1608
 1609
 1610
 1611
 1612
 1613
 1614
 1615
 1616
 1617
 1618
 1619

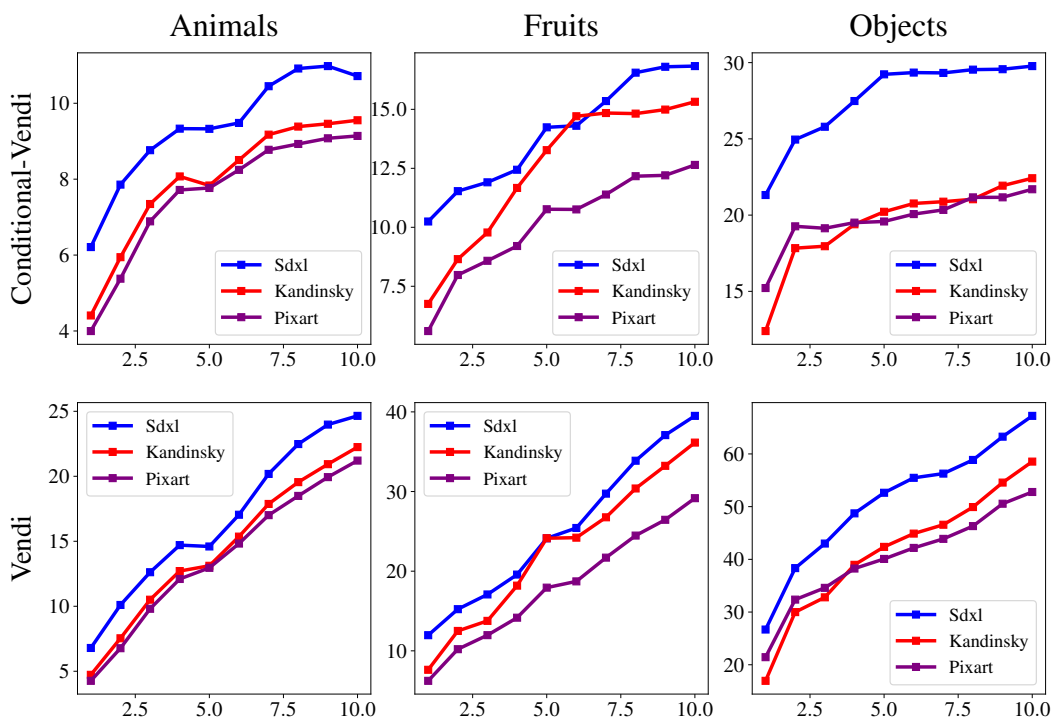


Figure 21: Evaluated (unconditional) Vendi and Conditional-Vendi scores of three text-to-image models in the category-based experiments with varying number of types within each of the categories: Animals, Fruits, Objects.

1620
 1621
 1622
 1623
 1624
 1625
 1626
 1627
 1628
 1629
 1630
 1631
 1632
 1633
 1634
 1635
 1636
 1637
 1638
 1639
 1640
 1641
 1642
 1643
 1644
 1645
 1646
 1647
 1648
 1649
 1650
 1651
 1652
 1653
 1654
 1655
 1656
 1657
 1658
 1659
 1660
 1661
 1662
 1663
 1664
 1665
 1666
 1667
 1668
 1669
 1670
 1671
 1672
 1673

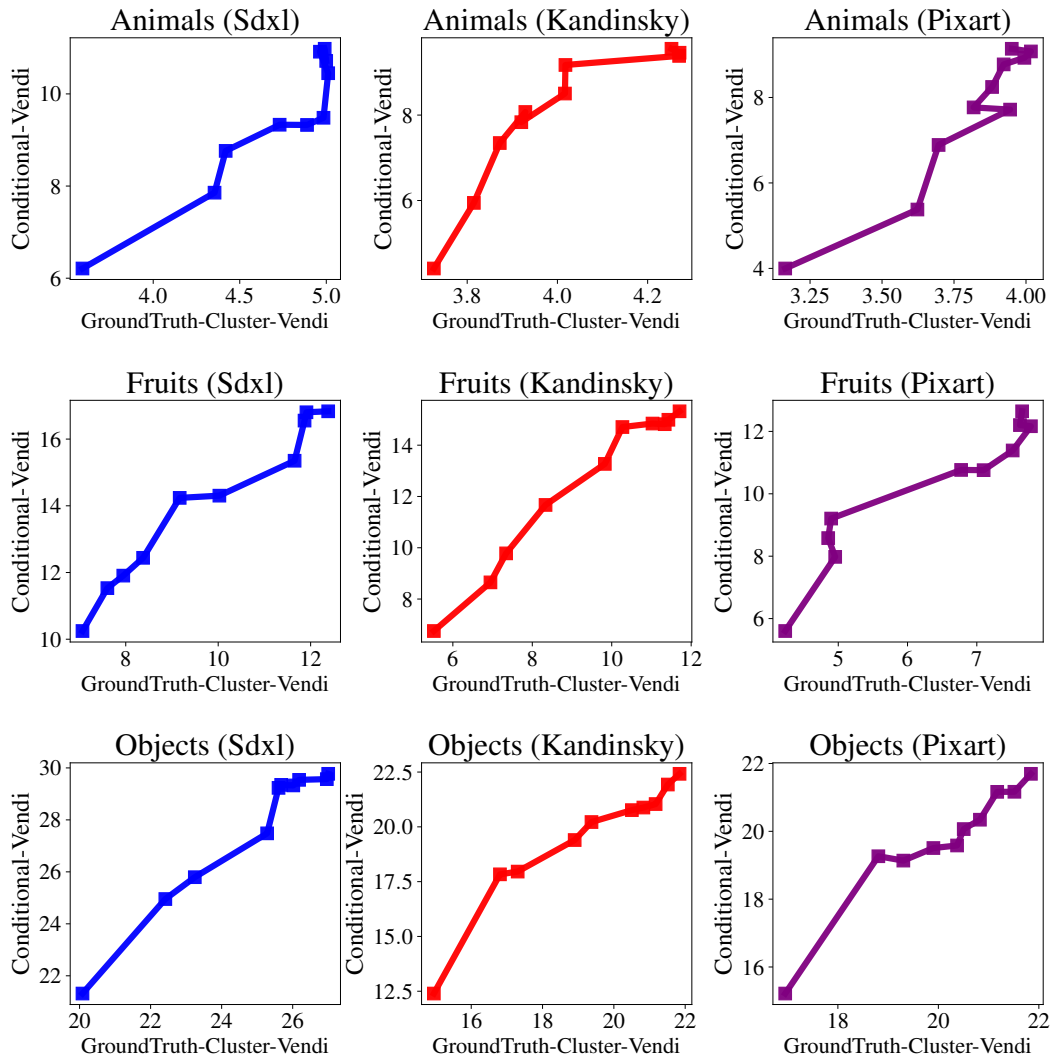


Figure 22: Comparing the Correlation of Conditional-Vendi with Groundtruth-Cluster-Vendi.

1674
 1675
 1676
 1677
 1678
 1679
 1680
 1681
 1682
 1683
 1684
 1685
 1686
 1687
 1688
 1689
 1690
 1691
 1692
 1693
 1694
 1695
 1696
 1697
 1698
 1699
 1700
 1701
 1702
 1703
 1704
 1705
 1706
 1707
 1708
 1709
 1710
 1711
 1712
 1713
 1714
 1715
 1716
 1717
 1718
 1719
 1720
 1721
 1722
 1723
 1724
 1725
 1726
 1727

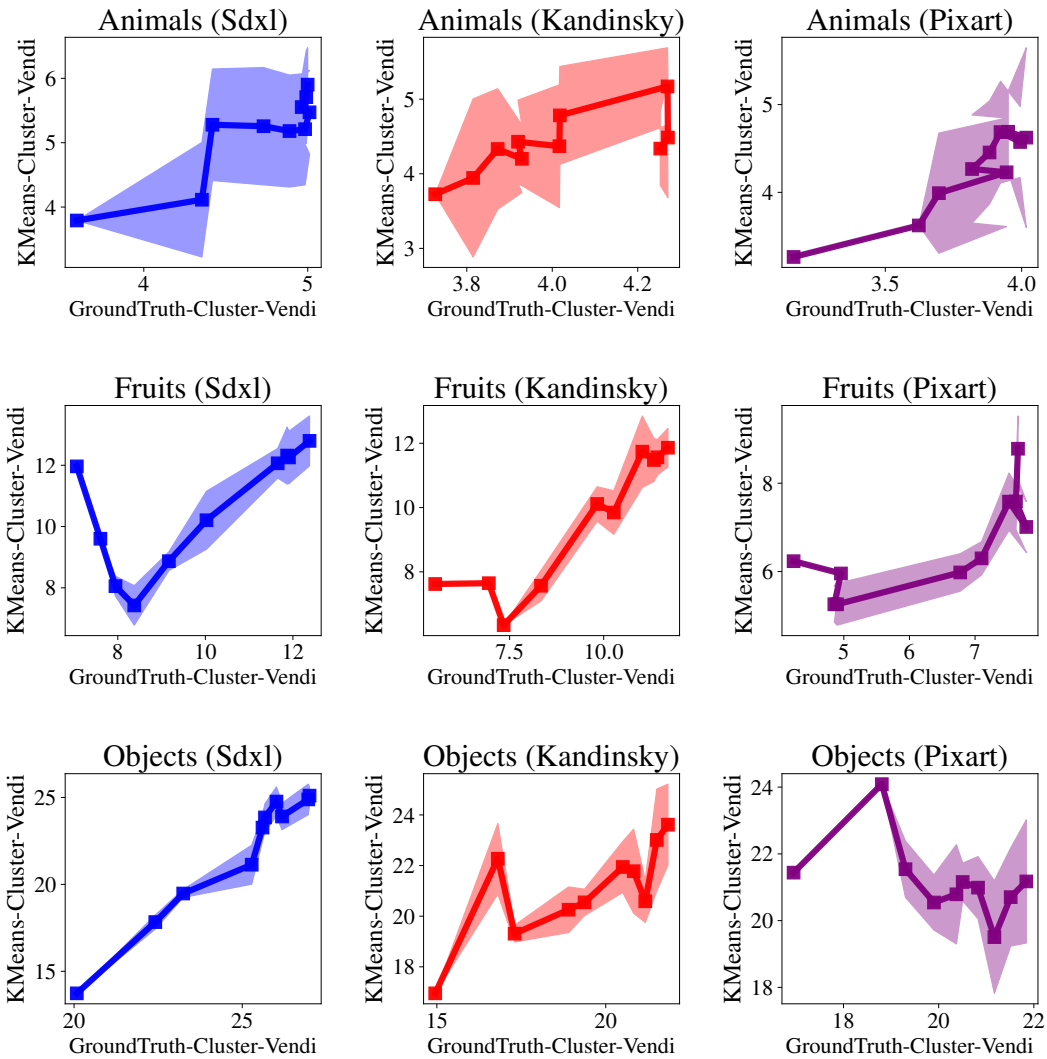


Figure 23: Comparing the Correlation of KMeans-Conditional-Vendi with Groundtruth-Cluster-Vendi.

1728
1729
1730
1731
1732
1733
1734
1735
1736
1737
1738
1739
1740
1741
1742
1743
1744
1745
1746
1747
1748
1749
1750
1751
1752
1753
1754
1755
1756
1757
1758
1759
1760
1761
1762
1763
1764
1765
1766
1767
1768
1769
1770
1771
1772
1773
1774
1775
1776
1777
1778
1779
1780
1781

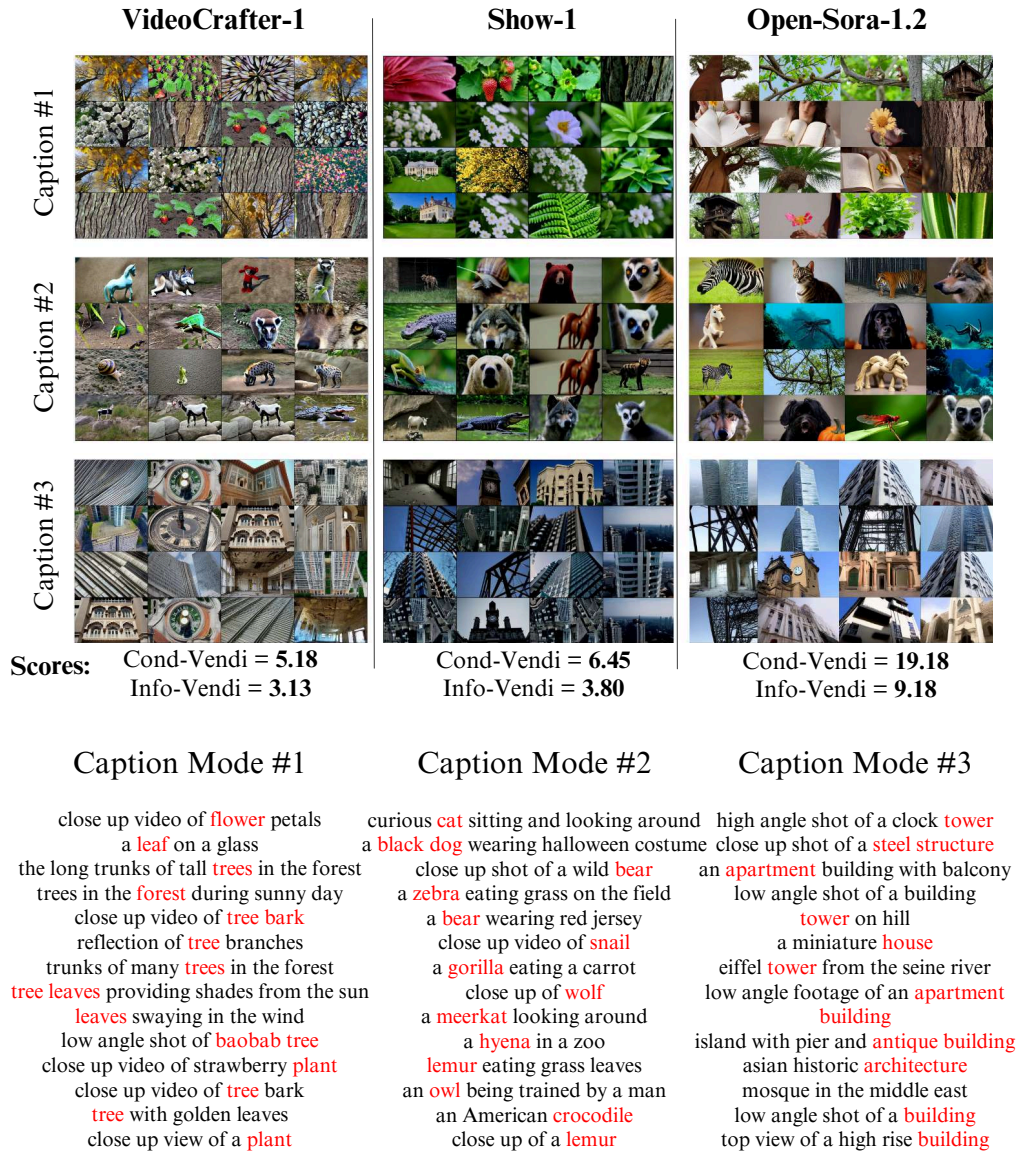


Figure 24: Measuring Conditional-Vendi and Information-Vendi for text-to-video models

1782
 1783
 1784
 1785
 1786
 1787
 1788
 1789
 1790
 1791
 1792
 1793
 1794
 1795
 1796
 1797
 1798
 1799
 1800
 1801
 1802
 1803
 1804
 1805
 1806
 1807
 1808
 1809
 1810
 1811
 1812
 1813
 1814
 1815
 1816
 1817
 1818
 1819
 1820
 1821
 1822
 1823
 1824
 1825
 1826
 1827
 1828
 1829
 1830
 1831
 1832
 1833
 1834
 1835

Algorithm 1 Conditional-Vendi and Information-Vendi

1: **Input:** Sample sets $\{\mathbf{x}_1, \dots, \mathbf{x}_n\}$ and $\{\mathbf{t}_1, \dots, \mathbf{t}_n\}$, Gaussian kernel bandwidths σ_i^2, σ_t^2 , order α .

2: **Compute kernel matrices:** $K_{\mathbf{X}} = \frac{1}{n}[k(\mathbf{x}_i, \mathbf{x}_j)]_{n \times n}$, $K_{\mathbf{T}} = \frac{1}{n}[k(\mathbf{t}_i, \mathbf{t}_j)]_{n \times n}$

3: **Perform eigendecomposition** on the $K_{\mathbf{X}}$, $K_{\mathbf{T}}$ and $\frac{1}{n}K_{\mathbf{X}} \odot K_{\mathbf{T}}$ matrices:

$$\{\lambda_1^{\mathbf{X}}, \dots, \lambda_n^{\mathbf{X}}\} \leftarrow \text{Eigendecomposition}(K_{\mathbf{X}})$$

$$\{\lambda_1^{\mathbf{T}}, \dots, \lambda_n^{\mathbf{T}}\} \leftarrow \text{Eigendecomposition}(K_{\mathbf{T}})$$

$$\{\lambda_1^{\mathbf{X}, \mathbf{T}}, \dots, \lambda_n^{\mathbf{X}, \mathbf{T}}\} \leftarrow \text{Eigendecomposition}\left(\frac{1}{n}K_{\mathbf{X}} \odot K_{\mathbf{T}}\right)$$

4: **Compute** $H_\alpha(\frac{1}{n}K_{\mathbf{X}})$, $H_\alpha(\frac{1}{n}K_{\mathbf{T}})$ and $H_\alpha(\frac{1}{n}K_{\mathbf{X}} \odot K_{\mathbf{T}})$ using their eigenvalues.

$$H_\alpha\left(\frac{1}{n}K_{\mathbf{X}}\right) \leftarrow \frac{1}{1-\alpha} \log\left(\sum_{i=1}^n (\lambda_i^{\mathbf{X}})^\alpha\right)$$

$$H_\alpha\left(\frac{1}{n}K_{\mathbf{T}}\right) \leftarrow \frac{1}{1-\alpha} \log\left(\sum_{i=1}^n (\lambda_i^{\mathbf{T}})^\alpha\right)$$

$$H_\alpha\left(\frac{1}{n}K_{\mathbf{X}} \odot K_{\mathbf{T}}\right) \leftarrow \frac{1}{1-\alpha} \log\left(\sum_{i=1}^n (\lambda_i^{\mathbf{X}, \mathbf{T}})^\alpha\right)$$

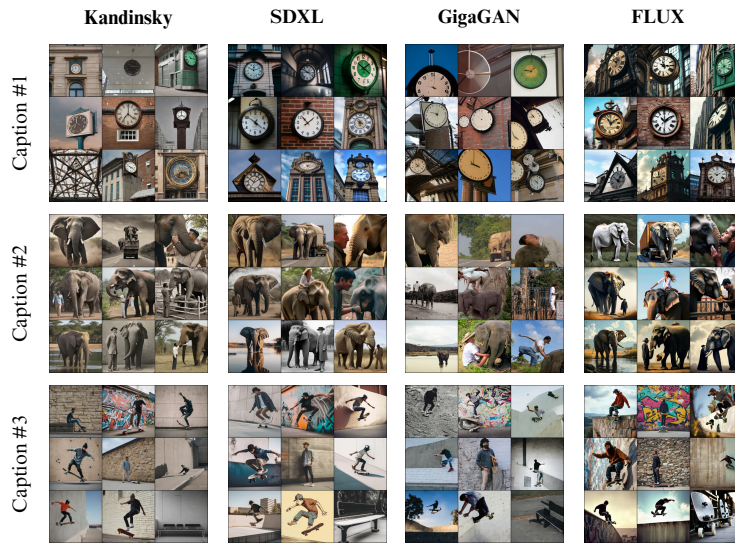
5: **Compute Conditional-Vendi and Information-Vendi**

$$\text{Conditional-Vendi}_\alpha(x_1, \dots, x_n | t_1, \dots, t_n) \leftarrow \exp\left(H_\alpha\left(\frac{1}{n}K_{\mathbf{X}} \odot K_{\mathbf{T}}\right) - H_\alpha\left(\frac{1}{n}K_{\mathbf{T}}\right)\right)$$

$$\text{Information-Vendi}_\alpha(x_1, \dots, x_n; t_1, \dots, t_n) \leftarrow \exp\left(H_\alpha\left(\frac{1}{n}K_{\mathbf{X}}\right) + H_\alpha\left(\frac{1}{n}K_{\mathbf{T}}\right) - H_\alpha\left(\frac{1}{n}K_{\mathbf{X}} \odot K_{\mathbf{T}}\right)\right)$$

6: **Output:** Conditional-Vendi and Information-Vendi

1836
1837
1838
1839
1840
1841
1842
1843
1844
1845
1846
1847
1848
1849
1850
1851
1852
1853
1854
1855
1856
1857
1858
1859
1860
1861
1862
1863
1864
1865
1866
1867
1868
1869
1870
1871
1872
1873
1874
1875
1876
1877
1878
1879
1880
1881
1882
1883
1884
1885
1886
1887
1888
1889



Caption Mode #1

- A building displaying a clock showing the time to be 6 o'clock.
- A clock hanging from the ceiling of a building.
- A large metal green clock hanging from the side of a building.
- A clock that is on top of a sign.
- A large clock mounted to a brick wall.
- A large clock hanging off the side of a tall building.
- A clock in near the triangular roof of a large building.
- A large clock and a sign on top of a building.
- A large clock mounted to the side of a building.

Caption Mode #2

- The elephant has a large white spot on its abdomen.
- The truck driver hauls an elephant down the highway.
- A man getting a kiss on the neck from an elephant's trunk
- A large elephant walking next to a man
- A woman in white shirt climbing onto an elephant.
- A man is leaning over a fence offering food to an elephant/
- A large elephant standing on the side of a lake.
- A man standing next to an elephant who stole his hat with it's trunk.
- A man standing near an elephant with its trunk outstretched.

Caption Mode #3

- A young man riding a skateboard on a stone wall.
- A man balancing on a skateboard in front of a graffiti covered wall.
- A man doing a trick on a wall with a skateboard.
- Bearded skateboarder maintains balance while skating up wall.
- A man standing next to a stone wall while holding a skateboard.
- There is a man skateboard on the side of a wall.
- a guy skate boarding on the edge of a wall
- A man on a skateboard is trying to jump over a wall.
- two black and white skate boards under a black steel bench

Figure 25: Effect of text kernel bandwidth on Conditional-Vendi and Information-Vendi scores

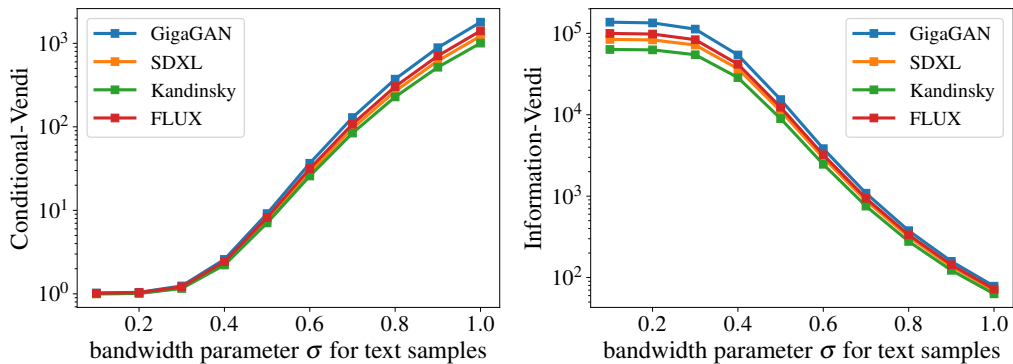


Figure 26: Effect of text kernel bandwidth on Conditional-Vendi and Information-Vendi scores